Utrecht University

MASTER'S THESIS

Study into the influence of support pore size on the structure and activity of Pd/C catalysts

Author:
Evan van Ommeren

Supervisors:
Wouter Lamme, *M. Sc.*
Prof. Dr. Ir. K.P. de Jong

A thesis submitted in partial fulfillment of the requirements for the degree of Master of Science

in the

Inorganic Chemistry and Catalysis group
Debye Institute for Nanomaterials Science

November 27, 2017

Abstract

Study into the influence of support pore size on the structure and activity of Pd/C catalysts

Palladium on carbon catalysts (Pd/C) are of great importance as a hydrogenation catalyst in chemical industry. In 2013, a quarter of drugs involved at least one hydrogenation step during their synthesis. Nevertheless, hydrogenation over Pd/C catalysts is not fully understood. Cinnamaldehyde hydrogenation is used as a model hydrogenation reaction, as cinnamaldehyde has two different sites that can be hydrogenated. Earlier research shows that the selectivity towards hydrogenation of the C=C or C=O bond is controlled by the palladium particle size. In this research, the influence of the pores in the carbon support on the palladium particles and the catalytic performance in the hydrogenation of cinnamaldehyde was explored. To this end, a method was developed using thermoporometry experiments to selectively impregnate pores of different sizes with a palladium tetraamine solution, which functions as a precursor to the palladium particles. These impregnations were performed by dry impregnation as overall impregnation method, partial impregnation to impregnate the smaller pores and micropore and small mesopore blocking with subsequent partial impregnation to selectively impregnate larger mesopores.
The final catalysts showed different selectivity according to intended impregnation location: palladium particles intended in small pores showed a higher selectivity towards hydrocinnamaldehyde formation and palladium particles in intended larger pores showed a slightly higher selectivity towards cinnamyl alcohol formation.

Acknowledgements

First of all, I would like to thank Wouter Lamme for supervising me in the past year and for the many interesting discussions we have had and the many ideas that came from these discussions. I am also grateful for your patience with me, especially when I came to you for the third time in a row to ask how a particular apparatus worked (especially the autoclave, which seemed a little daunting at first but the workings of which eventually proved to rely mostly on common sense). Also, I would like to thank Prof. Krijn de Jong for making it possible to do my research project in this group and teaching me so much about heterogeneous catalysis and about research in general. The discussions we had were not always easy for me, but were nonetheless inspiring and important to me. I would also like to thank Pascal Wijten for helping me out with the GC measurements, Marjan Versluijs-Helder for instructing me on the use of XRD and Mies van Steenbergen for getting me started on DSC and TGA. Finally, I would very much like to thank the people at BASF for the interesting discussions we have had and the very useful feedback I received on my work.

Contents

List of Figures

List of Tables

List of Abbreviations

AC	**A**ctivated **C**arbon
BET	**B**runauer **E**mmet **T**eller
DI	**D**ry **I**mpregnation
CNT	**C**arbon **N**ano**t**ube
DSC	**D**ifferential **S**canning **C**allorimetry
HAADF-STEM	**H**igh **A**ngle **A**nnular **D**ark **F**ield - **S**canning **T**ransmission **E**lectron **M**icropscopy
HDP	**H**omogeneous **D**eposition **P**recipitation
HSAG	**H**igh **S**urface **A**rea **G**raphite
NP	**N**ano **P**article
Pd	**P**alla**d**ium
Pd/C	**P**alla**d**ium on **C**arbon (catalyst)
PdTA	**T**etra**a**mmine**p**alla**d**ium
PSD	**P**ore **S**ize **D**istribution
PZC	**P**oint of **Z**ero **C**harge
(S)TEM	(**S**canning) **T**ransmission **E**lectron **M**icropscopy
TGA	**T**hermo **G**ravimetric **A**nalysis
TOF	**T**urn**o**ver **N**umber
XRD	**X**-**R**ay **D**iffraction

List of Symbols

A	Surface area	m^2
A_{BET}	BET surface area	m^2/g
h	Molar enthalpy	$\mathrm{J\,mol}^{-1}$
K_{GT}	Gibbs-Thomson constant	$\mathrm{nm\,K}$
m	mass	kg
P_l	Laplace pressure	Pa
r_p	Capillary radius	nm
T	Temperature	K
v	Molar volume	$\mathrm{m}^3/\mathrm{mol}$
V	Volume	m^3
γ	Surface tension	J/m^2
δ	Non-freezing layer	nm
θ	Contact angle	$^\circ$
ρ	Density	$\mathrm{kg}/\mathrm{dm}^3$
ϕ	Degree of pore filling	

Chapter 1

General introduction

1.1 Heterogeneous catalysis

Catalysis is employed in almost all large-volume chemical production. It could be argued that most man-made objects around us have been made using a heterogeneous catalyst at some point during production. Also, it is of great importance in the fuel production and conversion industries. Catalysts assist in chemical reactions to increase the reaction rate and selectivity towards the desired products, theoretically without being consumed. The overwhelming majority of catalysts used are heterogeneous catalysts, making them an important subject for study. These heterogeneous catalysts are in a separate phase from the reactants and products, e.g. solid/liquid, solid/gas or liquid/gas systems which makes it relatively easy to separate the products from the catalyst.

1.1.1 Supported metal catalysts

Often precious metals are used as solid state catalysts, making a high metallic surface area catalyst economically highly desirable as the catalytic activity takes place at the metal surface. These high metallic surface area catalysts are generally prepared as small nanoparticles of only a few nanometers in diameter, to maximize the surface area available for catalysis. However, these particles can not simply be loaded into a reactor. The particles would be hard to handle as the material would behave like a fine dust. Problems arising from using the bare metal nanoparticles include slow diffusion through the reactor in the case of gas-phase reactants and the fact that particles could easily sinter under elevated temperature and pressure as the metal particles are packed so closely together. This sintering of particles can also alter the selectivity of the reaction, due to particle size effects. This can be prevented by supporting nanoparticles on a solid support material which may have a porous structure in order to maximize the surface to mass ratio of the support.[1] In theory, a large support surface area combined with a large metal surface area would be ideal, with as much distance between individual metal nanoparticles as possible to prevent the particles from sintering.

1.2 Pd/C catalysts

Palladium on carbon (Pd/C) catalysts are of great importance as a hydrogenation catalyst in organic chemistry both on lab scale and on industrial scale syntheses.[2] They are used to convert unsaturated carbon compounds into saturated carbon compounds[3] but can also be employed towards reduction of aldehydes, nitro groups, nitriles and aromatics amongst others[4,5]. In 2013, a quarter of all drugs on the market had a hydrogenation step in their synthetic procedure,[6] making understanding of

the underlying catalytic processes important for optimizing these reactions. In many organic chemistry textbooks examples can be found for the employment of Pd/C catalysts in hydrogenation of (unsaturated) organic molecules. A large advantage of using carbon as a support for Pd catalysts is the facile recovery of palladium from spent catalysts[7]. The carbon as support can be readily oxidized to CO_2, leaving the palladium to be recycled for renewed use.

1.3 Production of Pd/C catalysts

In the procedure of creating Pd/C catalysts, several methods can be used to form palladium nanoparticles (NPs) on the carbon support surface. These methods include deposition precipitation, ion adsorption and dry impregnation[8].

1.3.1 Deposition precipitation

Deposition precipitation[9,10] is a two-step process which can be performed by first bringing the support into contact with a metal precursor solution. Depending on the precursor used, next an acid or base is added to adjust the pH of the solution to such pH that the metal salt is no longer soluble and precipitates. This may lead to large concentration gradients of the added acid or base, which can cause inhomogeneity in the distribution of the metal. A method to partially counteract this inhomogeneity is homogeneous deposition precipitation (HDP).[11] In this method instead of a simple base, urea is added and allowed to slowly decompose into ammonia and carbon dioxide by heating in order to raise the pH slowly and uniformly across the reaction mixture. This leads to a lowering of the precursor solubility resulting in highly uniform precipitation of the precursor onto the support. Next, the precursor is reduced, finally forming the metal nanoparticles. While the exact mechanistics vary from compound to compound and from support to support, this method is highly suitable to scale up due to its robustness.
A major issue with this method on industrial scale is the large amount of waste water to be treated, causing an increase in the cost of production. This is accompanied by the lack of control over where precipitation of the metal salt will occur. While statistically a certain amount will precipitate on the support surface, as this has a relatively high surface area on which to precipitate with respect to the reactor wall, a relatively large amount of the precipitate can either remain in suspension in the solvent, or precipitate on the reactor wall. The benefit in using this method however is the high metal loading that can be obtained while retaining small metal particles combined with narrow pore-size distributions.[12]

1.3.2 Ion adsorption

Ion adsorption[13] depends on the interaction between a charged surface and an oppositely charged adsorbent. In the case that little or no charge is present on the support surface, the surface may be functionalized with either acidic or basic oxygen or nitrogen containing functional groups. The choice between acidic or basic functional groups depends on the nature of the adsorbate. In the case of palladium adsorption, $[(NH_3)_4Pd]^{2+}$ (Tetraamminepalladium, PdTA) can be used for instance in the form of $(NH_3)_4Pd(NO_3)_2$. As this is a cationic species, the support surface needs to be negatively charged for adsorption of the PdTA onto the support. This can be attained by functionalization of the support surface with acidic functional groups, such as carboxylic or phenolic groups. The pH of the solution must be higher than the point

of zero charge of the support material to make sure the surface functional groups are deprotonated as otherwise the precursor cannot adsorb on the surface. This can be done by addition of a base prior to the addition of the precursor. The support can then be dried to remove the solvent. Next, the palladium nanoparticles are formed upon decomposition of the Pd-complex by a thermal treatment in an inert atmosphere. In order to reduce the palladium to metallic Pd(0) a source of electrons is needed which may be found in the carbon support. If a thermal treatment is not desired, a reducing agent such as sodium borohydride may be added to reduce the adsorbed palladium. The benefit in this method is that sodium borohydride can simply be added to the reaction mixture after the precursor has been allowed to adsorb to the support.

1.3.3 Dry impregnation

Dry impregnation is perhaps the most experimentally easy method to prepare a supported catalyst (see Figure 1.1), already being performed by Henry Deacon in 1868 in the preparation of supported copper catalysts for the synthesis of chlorine gas[12,14] as one of the earliest examples of supported catalysis. However, an easy to carry out preparation method does not mean that the physics occurring during impregnation is simple.
While in ion adsorption relatively large amounts of solvent are used in the adsorption step, this is not the case for dry impregnation[13,15] (DI). In this method only so much solvent, with the metal precursor dissolved, is used as to just fill the porous support structure. While in principle this sounds simple, this method still has considerable practical problems. It is often unknown whether the support pores are fully impregnated, risking to add too much of the impregnating liquid. If the pores are overfilled, a limited amount of the solvent may be present outside the pores. This means that metal will be deposited on the outside of the catalyst grains, which may lead to larger metal particles that can be prone to sintering, possibly altering the catalyst selectivity. On the other hand if pores are not sufficiently impregnated, the support may not be fully utilized leading to a lower activity. Decomposition of the precursor to form the final nanoparticles may be performed in the same manner as discussed in section 1.3.2.
The benefits to industry using dry impregnation are the small scale of waste production as no large amounts of solvent are needed in this technique and the limited number of operations needed to obtain the catalyst.[12] Also, the percentage of the metal deposited on the support instead of on the reactor wall is nearly 100%, which may be less in techniques such as ion adsorption.

Charge enhanced dry impregnation

Adsorption of the metal precursor may take place by electrostatic interactions between the support surface and the precursor.[16] The interactions between support and precursor are electrostatic in nature if the charges on the complex and surface are of opposite sign, as is the case in ion adsorption. These surface charges can, for instance, arise from oxygen- or nitrogen containing surface groups. By adding an acid or base to the impregnating solution for a high point of zero charge (PZC) or low PZC support respectively the support functional groups can be deprotonated or protonated in order for electrostatic adsorb to take place.
This technique is sometimes applied to obtain a maximum metal dispersion[16], but is not required for proper impregnation to occur; as in DI the pores are just filled

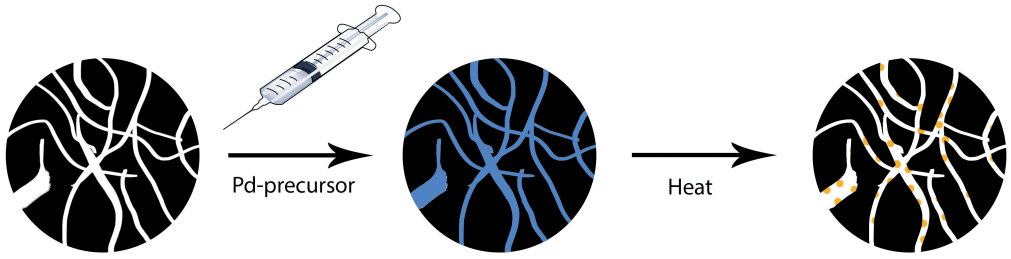

Figure 1.1: Impregnation of a solid support with a liquid precursor solution. First, the porous structure is filled with the precursor solution with no solution outside the grains. Next, via a heating program the support is first dried, precipitating the metal precursor on the pore walls. An activation or reduction step then forms the final metal nanoparticles inside the support pores.

without any additional liquid outside of the support all of the metal ions will enter the porous structure, so no metal precursor will be present outside the pore structure. Upon drying the precursor is deposited on the support. Activation of the metal precursor by heating then yields the metal particles inside the support pores as outlined in the paragraph above. An added benefit to charge enhanced dry impregnation (CEDI) is that metals deposited on the support cannot easily leach out in a reactor as the metal nanoparticles are somewhat anchored to the support surface.

1.4 Supports for Pd/C catalysts

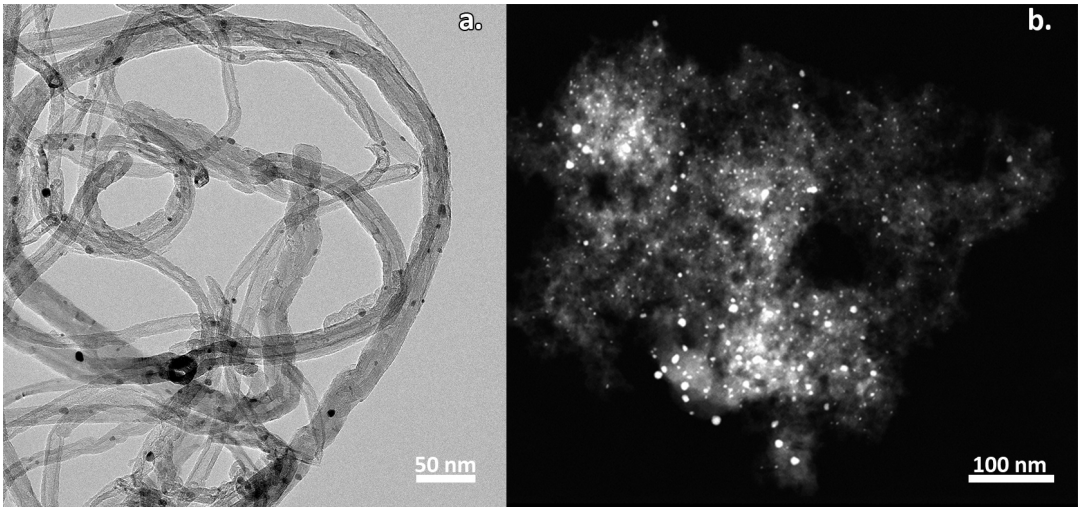

Figure 1.2: Pd/C catalysts on two different supports: **a.** TEM image of Pd on CNT support showing the individual CNT-strands supporting the Pd nanoparticles (black dots). **b.** HAADF-STEM image of Pd/AC (Norit GSX activated carbon) showing a relatively dense carbon structure with palladium particles as white dots.

Carbon supports can be numerous in differences, to name just a few: variations in pore size- and pore distributions can be found between different carbon materials- and sources. Also, variations in impurity levels such as iron, sulphur or sodium can be present, as well as different amounts of dopant species such as nitrogen and oxygen. While some variables, such as impurities cannot be easily controlled as

they are (partially) dependent on the carbon source used, others can be optimized for a particular catalyst. For research purposes, carbon nanotubes (CNT) are often employed.[17] These supports offer the possibility to accurately study Pd/C catalysts without the effects of diffusion limitations being present as these support pores mainly consist of macropores and large mesopores. In Figure 1.2 two Pd/C catalysts are depicted with different supports. Left, a carbon nanotube supported catalyst with a relatively open pore structure and right a relatively dense activated carbon supported catalyst.
In industrial applications cost considerations are an important factor in deciding the support used for the catalyst at hand. Activated carbons (AC), which is a pyrolysis product, offers this low cost. However purity levels and pore structure can vary greatly in these carbon materials; these carbons often show a complex porous structure containing a varied micro-, meso- and macroporous structure.[18]
Carbon xerogels may be employed to avoid most of aforementioned problems. These synthetic carbons have a narrow pore size distribution with a pore size that can be tuned by altering the synthesis conditions.[19] These may thus form a practical model for research into the influence of micropores on catalyst formation and activity, however they are prohibitively expensive to use as a support on an industrial scale.

Support functionalization Metal particles may not always be able to properly attach to unfunctionalized carbon supports. This may lead to coalescence of the metal particles or leaching during the catalyst lifetime, when the metal particles show a weak interaction with the carbon support.[1]
In order to properly attach the metal nanoparticles to the support surface, functional groups are required on the support surface, which are also required for charge enhanced dry impregnation. On a small lab scale, these surface functionalizations can be introduced by refluxing of the support in a nitric acid solution, creating a multitude in acidic functional groups on the support surface ranging from alcohol- to carboxyl groups.

1.5 Previous work

In his Bachelor's thesis,[20] Den Brave researched the behaviour of water confined in porous high surface area graphite (HSAG). His research was performed by impregnating samples of HSAG to a different extent with water and subsequently measuring the melting point of the pore water for this sample using Differential Scanning Calorimetry (DSC). Next, to determine the exact amount of water present in the sample, Thermogravimetric Analysis (TGA) was performed. It was found that when only a small fraction of the pore volume of an HSAG sample was filled, the observed melting point would be considerably lower than when an HSAG sample would be impregnated to a larger extend. This means that water will go to the smallest pores present upon addition, as the melting point of water confined in pores is a function of the pore radius. A qualitative relationship can thus be made for the extent of pore filling and the pore radius that was filled.

Chapter 2

Aim of the project

Activated carbons, as explained in the first chapter, are an important class of supports in industry and therefore an interesting subject of study. However, the properties of activated carbons are very diverse, with purity levels and pore structure varying greatly,[18] even between batches of the same type of activated carbon. Not much is known about the influence of the porous structure of activated carbons on Pd/C catalysts. This is probably in large part due to the great variation in pore structure between activated carbons. In this work, an attempt is made to understand the influence of the porous structure of activated carbons on catalyst activity and selectivity in Pd/C catalysts.
In order to study the catalytic activity of the palladium catalyst in the micro- and mesopores of the carbon support, two main questions needed to be answered. Can we gain control over where in the catalyst support the palladium particles are formed and can we measure this? And does the location of the metal particles have an effect on the performance of catalytic hydrogenation of cinnamaldehyde? In this thesis, a method is explored using selective impregnation combined with thermal analysis and catalytic testing to explore these goals.

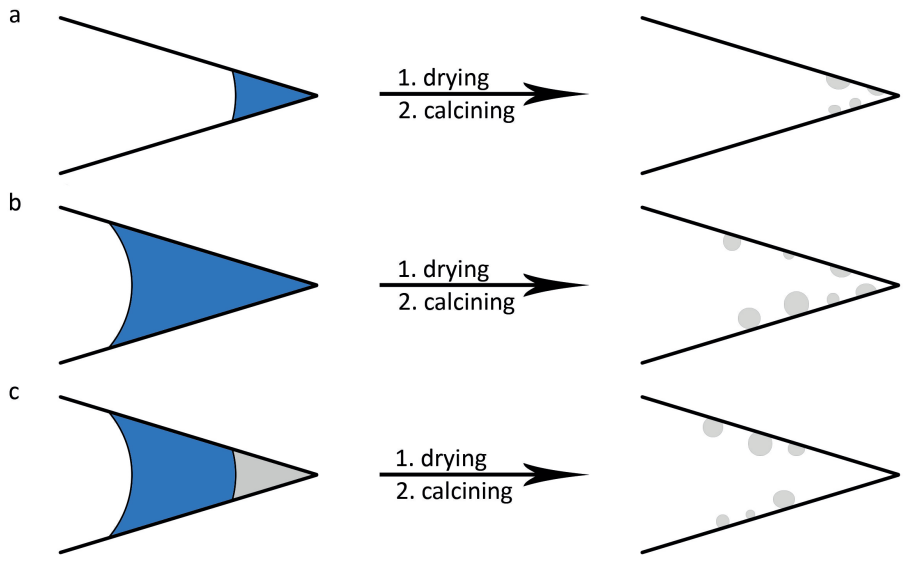

Figure 2.1: Impregnation of the porous support **a.** in micro- and small mesopores **b.** homogeneous distribution of all pores by full impregnation **c.** into large mesopores by first blocking small pores. Porous support schematically depicted as a wedge, representing a continuous distribution of pore sizes going from large to small pores.

2.1 Selective impregnation

2.1.1 Impregnation into micropores and small mesopores

If a catalyst support is properly impregnated with a liquid by dry impregnation, it is reasonable to assume that a relatively uniform distribution of metal particles on the support surface is obtained, irrespective of the pore size distribution of the support. Classically, this is a highly beneficial characteristic in a supported catalyst, as this allows for a high total surface area of the active metal which facilitates optimal dispersion and stability of the metal resulting in an optimal catalyst activity. However, when a homogeneous distribution of the metal is obtained, metal particles may also be present in pores less readily accessible to the substrate in a reaction catalysed by this catalyst. This may be due to diffusion limitations or pore blockage by the metal particles resulting in a lower catalyst activity. In order to study this effect, impregnation may be performed selectively into support pores of a certain diameter. Partial impregnation of carbon supports using water was studied by Daniël den Brave[20]. In this study, partial impregnation of carbon supports will be further explored to study the possibility to exclusively form metal NPs in micropores as shown in Figure 2.1a. However, it is not known to what extent deposition of the metal precursor occurs before the solution reaches the micropores. A possibility is that precursor deposition starts to occur as soon as the precursor solution comes into contact with the support, resulting in an unintended homogeneous distribution of the metal over the support.

2.1.2 Impregnation into large mesopores and macropores

Partial impregnation may allow control over impregnation location. If only the micropores are to be impregnated, incomplete impregnation of the support may be used to only fill these micropores due to capillary action. A modification of this strategy may offer a possibility to selectively impregnate larger (meso)pores in the support with a metal precursor solution.
To exclude the precursor from the micropores, it may be possible to block the micropores by filling the pores with another substance which is preferably not miscible with the precursor solution. After that, the mesopores can be impregnated with the precursor solution. Upon drying and calcination, metal crystallites may selectively be formed in the mesoporous structure as depicted in Figure 2.1c. Care must be taken that the precursor does not bleed into the micropores. Another likely bottleneck is that upon drying of the impregnated support, the precursor-containing water should evaporate before the solvent in the micropores. Thus, as pore blocking agent a solvent with a boiling point well above that of water should be chosen.

2.2 Catalyst synthesis and testing

Several catalysts will be made using the principles outlined above. Also, catalysts will be prepared by full impregnation (Figure 2.1b) to compare the activity and selectivity of these catalysts to those prepared by selectively impregnating the support. In order to study the difference in activity and selectivity for the active metal catalyst particles confined in pores of different widths, the catalysts need to be tested. Catalytic testing will be performed for the hydrogenation of cinnamaldehyde, as this α,β-unsaturated aldehyde has two different π-bonds (Figure 2.2) with different reactivities to be hydrogenated. In this study the difference in conversion and selectivity will be studied for palladium particles in different locations in the support pores.

Earlier studies[21] show that the palladium particle size can have a big impact on the conversion and selectivity of the reactant, which also has to be taken into account when studying the effect of palladium particle-location.

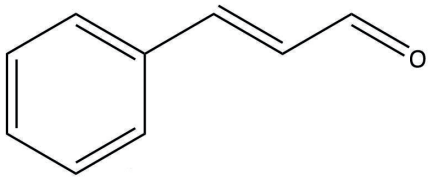

Figure 2.2: The α,β-unsaturated aldehyde cinnamaldehyde. Either the C=O, C=C or both can be hydrogenated by hydrogen using a Pd/C catalyst.

Chapter 3

Selective impregnation

3.1 Introduction

In order to form catalysts with Pd particles located in pores of a specific size, a method was developed to selectively impregnate the palladium precursor in pores of different widths. Den Brave[20], as explained in section 1.5, studied the melting- and freezing behaviour of water confined in pores of high surface area graphite and carbon xerogels. He showed that upon impregnation, water first fills the smaller pores before larger pores were filled. In this work, this relation was further explored for the impregnation of a carbon support with an aqueous solution of $(NH_3)_4Pd(NO_3)_2$ (PdTA) and a quantitative relationship was made between the impregnation volume, average pore radius and melting point depression.

3.2 Theoretical considerations

3.2.1 Dry impregnation

The technique of catalyst preparation by dry impregnation consist of several main steps: the impregnation itself, drying and activation, optionally followed by reduction of the metal catalyst by hydrogenation. In this chapter, the impregnation step is considered.
Dry impregnation is commonly described as filling the support pores with just enough liquid as to just fill the pores without liquid being present on the outside of the pores. Additionally, underfilled pores should be avoided to obtain the highest dispersion of the catalytically active metal, theoretically leading to a maximum catalyst activity if the support pores are of uniform size. If the impregnating liquid is wetting the support, capillary suction will force the liquid into the pores as described by the Laplace equation.[22] This relates the Laplace pressure P_l, which is the pressure difference between the inside and outside of the liquid, to the contact angle of the liquid, liquid surface tension and pore radius via:

$$P_l = \frac{2\gamma \cos\theta}{r_p} \tag{3.1}$$

in which γ is the surface tension in (N m^{-1}), θ the contact angle of the liquid with the capillary wall and r_p the capillary or pore radius in meters. The equation shows that with decreasing pore radius the Laplace pressure rises if the liquid is sufficiently wetting towards the capillary walls ($\theta < 90°$). As the support pores are in the size range of nanometres, or 10^{-9} meters, the pressures exerted can become considerably large thus forcing the liquid into the pores.
A possible risk, present when bringing a support into contact with a liquid is that the

mechanical strength of the support is not high enough to withstand the large forces acting on the support when pockets of air, locked in upon impregnation, escape the porous support. This may be easily prevented by first bringing the support into vacuum, after which the impregnating solution is added. This may also prevent atmospheric water from being present in the reaction when using a hygroscopic support. Practically, this means that prior to impregnation the support is dried under vacuum at an elevated temperature. The impregnation solution containing the support is then added under vacuum. A magnetic stirrer is added to agitate the impregnated support when the liquid is equilibrated.

Adsorption of dissolved precursor

Adsorption of the metal precursor may take place at two different instances after impregnation. The dissolved metal precursor may adsorb on the support surface immediately after impregnation due to electrostatic interactions between the support surface and precursor. This is especially important in the case of charge enhanced dry impregnation and may lead to adsorption primarily occurring at the boundary of the support grains, thus obtaining an inhomogeneous distribution of the metal on the catalyst grains. Else, when the interaction between the support surface and metal precursor is less strong the precursor may stay in solution while the solvent is evaporated until the precursor solution is saturated. Continuing the evaporation of the solvent, the metal precursor is deposited on the support surface which leads to a homogeneous distribution of the metal across the entire support surface.

3.2.2 Thermoporometry

As dry impregnation is used as catalyst preparation method, requiring a solution of the metal precursor, for the synthesis of catalysts and the catalysts are used in liquid-phase reactions, it is convenient to measure the pore size in an aqueous environment. As explained in section 3.4.1, the pores in the carbon supports used swell upon impregnation with an aqueous solvent, resulting in different pore sizes than those obtained by N_2-physisorption. This means that N_2-physisorption cannot be reliably used to determine the pore size distribution of the catalyst under preparation or in-use, as the catalyst will be in contact with a liquid and thus will have a different pore volume than the dry support as measured in N_2-physisorption. A method is thus required to determine the pore sizes present in the liquid-containing support. Thermoporometry can be used to study the porous structure of solid materials,[23] in this case carbon supports. This technique is based on the Gibbs-Thomson effect which describes the freezing- and melting behavior of liquids confined in pores. Thermoporometry is carried out using a standard Differential Scanning Calorimeter. Differential Scanning Calorimetry (DSC) is commonly used to measure the heat flow upon heating or cooling of a sample and has multiple applications in materials science and pharmaceutics, for instance in quality control.[24] However, the observed heat flow can also be used to measure the freezing- and melting temperature of a high heat capacity liquid such as water. When measuring the heat flow of a liquid upon melting using DSC, a decrease in the heat flow would be observed at the meltingpoint of the liquid in question, with the integral of the curve being the total enthalpy of melting for the sample mass. Upon confinement of a liquid in a cylindrical pore of radius R, the melting point of the liquid changes by

$$\Delta T_{\mathrm{m}} = T_{\mathrm{mb}} - T_{\mathrm{m}} = \frac{2T_{\mathrm{mb}}(\gamma_{\mathrm{ws}} - \gamma_{\mathrm{wl}})v_{\mathrm{l}}}{r_{\mathrm{f}} \cdot \Delta_{\mathrm{sl}} h} \tag{3.2}$$

In this equation T_{mb} and T_{m} are the melting temperature of the bulk liquid and confined liquid respectively, γ_{ws} and γ_{wl} are the wall-solid and wall-liquid interfacial tensions. v_{l} is the molar volume of the liquid, $\Delta_{\mathrm{sl}}h$ is the molar enthalpy of melting and r_{f} the radius of the frozen liquid inside the pores. In this case it can be assumed that $r_{\mathrm{f}} = r_{\mathrm{p}}$ and thus that the radius of the frozen liquid is equal to the pore radius. This formula essentially shows that when a liquid is confined in a porous structure, the melting temperature of this liquid is lowered by a value of ΔT_{m} in the case that $\gamma_{\mathrm{ws}} - \gamma_{\mathrm{wl}} > 0$, meaning that the liquid is wetting towards the wall. When the liquid is fully wetting the pore wall, the equation becomes $\gamma_{\mathrm{ws}} - \gamma_{\mathrm{wl}} = \gamma_{\mathrm{sl}}$ and the Gibbs-Thomson equation becomes:

$$\Delta T_m = T_{\mathrm{mb}} - T_m = \frac{2T_{\mathrm{mb}}\gamma_{\mathrm{sl}}v_{\mathrm{l}}}{r_{\mathrm{f}} \cdot \Delta_{\mathrm{sl}}h} = \frac{K_{\mathrm{GT}}}{r_{\mathrm{f}}} \tag{3.3}$$

With K_{GT} the Gibbs-Thomson constant, which is a function of the bulk melting temperature T_{m}, the molar volume v_{l} and the molar enthalpy of melting $\Delta_{\mathrm{sl}}h$ of the liquid. The parameter K_{GT} provides a straightforward relationship between the change in melting temperature and pore radius.
A study performed by Schmidt *et al.*[25] into pore size determination on mesoporous MCM-41 found that not all pore water freezes. Instead, a non-freezing water layer is formed on the pore wall due to strong interactions with the pore surface. This requires a modification of the Gibbs-Thomson equation. The equation then becomes:

$$\Delta T_{\mathrm{m}} = T_{\mathrm{mb}} - T_{\mathrm{m}} = \frac{K_{\mathrm{GT}}}{r_{\mathrm{p}} - \delta} \tag{3.4}$$

With r_{p} the total pore radius of the support and δ the non-freezing water layer. Rewriting the equation to find the pore radius r_{p} gives the function in its final form:

$$r_{\mathrm{p}} = r_{\mathrm{f}} + \delta = \frac{K_{\mathrm{GT}}}{T_{\mathrm{mb}} - T_{\mathrm{m}}} + \delta \tag{3.5}$$

In thermoporometry measurements on carbon xero-, cryo- and aerogels, Veselá *et al.*[26] used the value of $K_{\mathrm{GT}} = 52$ nm K, which was first determined by Schreiber *et al.*[27] for the melting and freezing in ordered mesoporous silica materials. As K_{GT} is only a function of the contact angle between the liquid and solid and melting properties of the liquid, this value can be used for other (carbon based) materials, assuming that the wettability of the solid is not changed. In this research, Veselá used a value of 0.8 nm for the non-freezing layer thickness δ for their measurements based on an estimation made by Yamamoto *et al.*[28].

3.2.3 Pore volume determination

In order to calculate the extent of pore filling of the porous support, the water accessible pore volume can be determined by impregnating the support up to such extent that the pores are fully impregnated, without bulk water being present. The degree of pore filling for a porous material is determined by the simple mathematical relationship:

$$\phi = \frac{V_{\mathrm{l}}}{V_{\mathrm{p}}} \tag{3.6}$$

In which V_{l} is the total volume of the impregnating liquid and V_{p} the total pore volume of the porous solid. As it is not possible to directly measure the volume of

the impregnating solution, the equation can be written as:

$$\phi = \frac{m_{\mathrm{l}}}{m_{\mathrm{s}} \cdot \rho_{\mathrm{l}} \cdot v_{\mathrm{p}}} \tag{3.7}$$

With m_{l} the measured mass of the liquid obtained from TGA, m_{s} the mass of the porous support, ρ_{l} the density of the impregnating liquid and v_{p} the pore volume of the sample. At $\phi = 1$, the pores are completely filled, and thus the volume of the impregnating liquid V_{l} (usually water) is equal to the total pore volume V_{p}. Using the equation above, it is easy to calculate the extent of impregnation in the case of incomplete pore filling, used to obtain a relationship between extent of pore filling and the pore size.

3.2.4 Blocking of micropores and small mesopores

In order to be able to selectively impregnate the larger pores of the support with the PdTA solution, we studied whether it was possible to selectively block the micropores and smaller mesopores with a pore blocking agent. Several requirements for a possible pore blocking agent were formulated to maximize the possibility of a positive outcome:

- Good wettability of support
- (largely) immiscible with water
- preferably a melting point higher than water

Three different pore blocking agents were selected to be tested as pore blocking agents: toluene, cyclohexanol and phenol. Toluene was chosen largely because of its immiscibility with water. Also, it was suspected that toluene would show favourable interactions with the pore surface which may aid in the adsorption into the micropores. Cyclohexanol was selected as a possible pore blocking agent as it is a small molecule which has a low solubility in water (3.60 g cyclohexanol in 100 mL water at 20 °C), and has a melting point of 25 °C. Also, it is relatively polar due to the $-$OH group, which may aid in wetting of the support surface if there are polar groups present. Finally, phenol (melting point: 40.5 °C) was tested as a pore-blocking agent as the higher melting point may allow for a more controlled manner of addition to the support. Other benefits of phenol as a pore blocking agent include the high boiling point of 181 °C, which makes it possible that impregnated or infiltrated phenol only evaporates from the support after all the water has evaporated in the drying step of catalyst preparation.

Melt infiltration

In order to fill the micropores and small mesopores of the support with the pore blocking agents, two techniques were explored: dry impregnation and melt infiltration. Melt infiltration has the advantage that a substance in its room-temperature solid state can be infiltrated into the porous structure without prior melting of the compound in question. In order to homogeneously infiltrate the support grains, the solid can be ground to obtain small, millimeter sized, crystallites. These can then be mixed as solid through the support, subsequent heating is used to melt the solid, after which capillary- or externally applied forces force the molten solid into the pores.

3.3 Experimental procedure

3.3.1 Materials

High Surface Area Graphite (HSAG) Timrex HSAG500 (Timcal) was used as carbon support. Tetraamminepalladium (II) nitrate (PdTA) solution, 99.9% (metals basis, Pd content 5.0%) was acquired from Alfa Aesar. Phenol (99%, extra pure) was obtained from Acros Organics. In all experiments MilliQ demineralized water was used, unless stated otherwise.

3.3.2 Support pretreatment

Samples were prepared by putting 300 milligrams of HSAG500 in a 2-necked 100 mL round-bottom flask equipped with a septum, valve and magnetic stirrer. The carbon was dried by heating to 170 °C under vacuum for two hours, applied using a heating mantle and electric vacuum pump. After two hours, the sample was allowed to cool to room temperature retaining the vacuum after which the carbon could be used for further experiments.

3.3.3 Dry impregnation

Dry impregnation was used as impregnation method for water and the tetraamminepalladium solution. In experiments without prior pore blocking the dried carbon prepared via the method described in 3.3.2 was impregnated using the PdTA solution via the description below. When using the porous carbon with blocked micropores and small mesopores prepared via the methods described in 3.3.4 or 3.3.5, water was used as impregnating liquid.
A syringe was used to add the liquid to be impregnated to the carbon without breaking the vacuum. The liquid was added instantly, followed with between ten minutes and two hours of stirring as homogenization time. After addition of the liquid, it was checked that the carbon did not look wet, which is an indication that no liquid is present outside the pores. In the experiments where more than an hour homogenization time was allowed, the vacuum was removed after several minutes by opening and closing the valve of the round bottom flask. This was done as otherwise the impregnating liquid could exit the pores, forming condensation on the top of the round-bottom flask.

3.3.4 Micropore blockage via dry impregnation

Micropore blockage via dry impregnation was performed using toluene and cyclohexanol as pore blocking agents. After drying the support as described in 3.3.2, the pore blocking agent was added using a syringe to the carbon without breaking the vacuum. The liquid was added instantly, followed with two hours of stirring as homogenization time. The carbon could then be used to be impregnated with water via the method described in 3.3.3.

3.3.5 Micropore blockage via melt infiltration

Melt infiltration was performed to selectively block micropores in the carbon support using phenol. This was performed by first drying the carbon as described in section 3.3.2. As the phenol, the pore-blocking agent, is a solid at room temperature the valve had to be removed to add the phenol, meaning that some atmospheric

water vapour may enter the system and condense on the carbon sample. Therefore the flask was filled with N_2 prior to addition of the phenol. This was done via an N_2 filled balloon attached to the valve which was quickly opened and closed again in order to keep a closed system. The amount of water vapour entering the system in this manner was taken as negligible as the density of nitrogen gas should prevent thorough mixing with air during the brief time of phenol addition. Upon addition, the millimeter-sized phenol crystals were first stirred through the support material with a magnetic stirrer to improve the homogeneous distribution of the pore blocking agent over the support grains. Next, the sample was heated by putting the round-bottom flask in a waterbath set to 55 °C to allow infiltration of the phenol into the support pores. After two hours stabilization time, the waterbath was removed and the round-bottom flask allowed to cool down to room temperature. Finally, the carbon could be used to be impregnated with water via the method described in section 3.3.3.

3.3.6 Thermoporometry measurements

Thermoporometry measurements are carried out using Differential Scanning Calorimetry on a TA Instruments Q2000 DSC. After impregnation of the carbon support several samples were taken and put into a DSC pan (40 µL, Tzero Pans, aluminium, TA Instruments) at room temperature, which was then hermetically sealed with a lid to prevent evaporation from and condensation to the carbon sample. For a typical measurement, between 5 and 10 mg of sample was used. As reference an empty pan (hermetically sealed) of similar weight was used. Samples were cooled to −55 °C. After holding the temperature at −55 °C for 10 min to stabilize the sample, the sample was heated to 20 °C. The rate of cooling and heating was 1 °C/min, providing a reasonable resolution if multiple clearly defined melting peaks would be observed.[26,27]

3.3.7 Thermogravimetric analysis

Thermogravimetric analysis (TGA) was performed to determine the amount of liquid present in carbon samples after performing DSC, using a Q50 TGA apparatus from TA Instruments. The lids of the pans used in DSC were carefully pierced using a needle, making sure not to touch the sample, prior to performing TGA to allow water vapour to be expelled during the measurement.
The pans were heated under a nitrogen flow of 60 mL per minute at a rate of 4 °C/min to 500 °C subsequently holding the temperature at 500 °C for 2 hours to make sure that the Pd-complex was fully decomposed. From this, the total amount of material impregnated into the support can be calculated as explained in Appendix A.

Measurement of pore-blocking agents

As TGA is used to track a weight change upon (partial) evaporation of a sample, it can be used to track the evaporation of multiple compounds, as long as the difference between the boiling points of the compounds are large enough. By calculating the derivative of the weight change, the start and end points for evaporation of different compounds were calculated.

3.4 Results and discussion

3.4.1 Pore volume determination of carbon supports

The value obtained for the water accessible pore volume of HSAG500 deviates significantly from the pore volume obtained through N_2 physisorption. For nonfunctionalized HSAG 500 the BJH pore volume given by the desorption curve in N_2-physisorption is 0.512 cm^3/g for pores between 1 and 300 nm in diameter. However, the water-accessible pore volume of HSAG 500 was found to be 1.1 cm^3/g. This water-accessible pore volume was confirmed by first preparing a carbon sample by impregnation with water. Next, the impregnated sample was measured using DSC. It was observed that the melting point of the confined water approached that of bulk water, thus meaning that the pores were completely filled or even slightly overfilled. As a final check to confirm the amount of water in the DSC sample, the amount of water in the carbon sample was measured using TGA, confirming the water-accessible pore volume to be 1.1 mL per gram of carbon.
This discrepancy between N_2 physisorption and the water-accessible pore volume suggests that the open structure of carbon is not rigid. Instead, the pores in carbon may be able to expand to allow more room for the contacting liquid, thus slightly moving the solid carbon within a particle apart. This is important as it may influence the catalytic activity of the final catalyst. Using the techniques here, it is not possible to say how exactly these carbon structures swell and thus which pores see an increase in size.

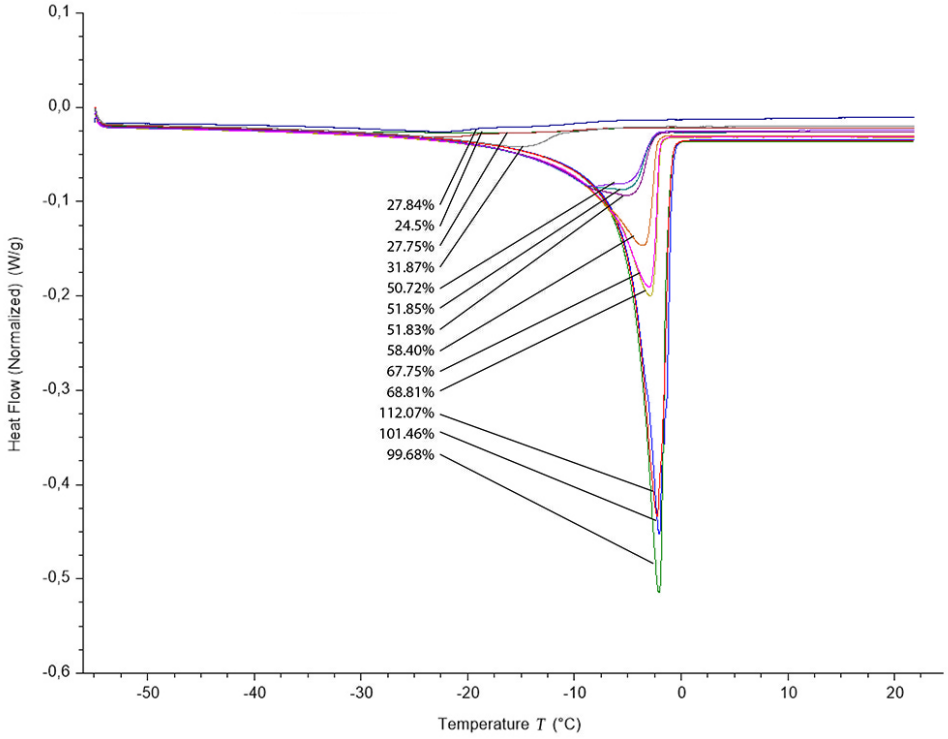

Figure 3.1: DSC thermogram displaying the shift in melting point of the tetraamminepalladium solution in pores of different sizes. On the x-axis is the temperature displayed in °C and on the y-axis the heat flow measured for the sample, which is normalized to the total weight of the sample (liquid plus carbon support).

3.4.2 Melting behaviour of palladiumtetraamine in porous HSAG

High Surface Area Graphite HSAG 500 was impregnated up to different extents by dry impregnation via the method described in section 3.3.3. Using DSC (Figure 3.1), a melting peak onset and melting peak maximum were determined for different ϕ ranging from 0.24 to 1.1. For none of the samples a melting peak onset was found above -0.94 °C, as well as no observed melting peak maxima above -2.01 °C indicating that no bulk liquid was present in these samples. On the left from the peak maxima fronting is observed. It is especially interesting to note that for full impregnations and the slightly overfilled impregnation (ϕ between 0.99 and 0.112), the fronts fully encompass the peaks of the partially impregnated samples (ϕ between 0.24 and 0.68). Porous materials containing pores of uniform pore size (narrow pore size distribution) would have sharp peaks without any fronting, as suggested by the Gibbs-Thomson equation. It was thus concluded this fronting is caused by the continuous distribution of pore sizes within the samples.

Melting behaviour in overfilled pores

Samples with slightly overfilled pores ($\phi > 1$), showed a similar peak in melting point, as can be seen in Table 3.1. It is interesting to note that the Gibbs-Thomson equation for the pore radii where the pore water is located, give near-meaningless results as resolution of the peak melting temperatures is not adequate this close to the bulk melting temperature of water. It is important to note that the Gibbs-Thomson equation (3.5) applies to cylindrical pores. While the disordered nature of activated carbon may suggest an array of different types of pores, the simplification was made that the water-logged pores assume a near-cylindrical conformation.

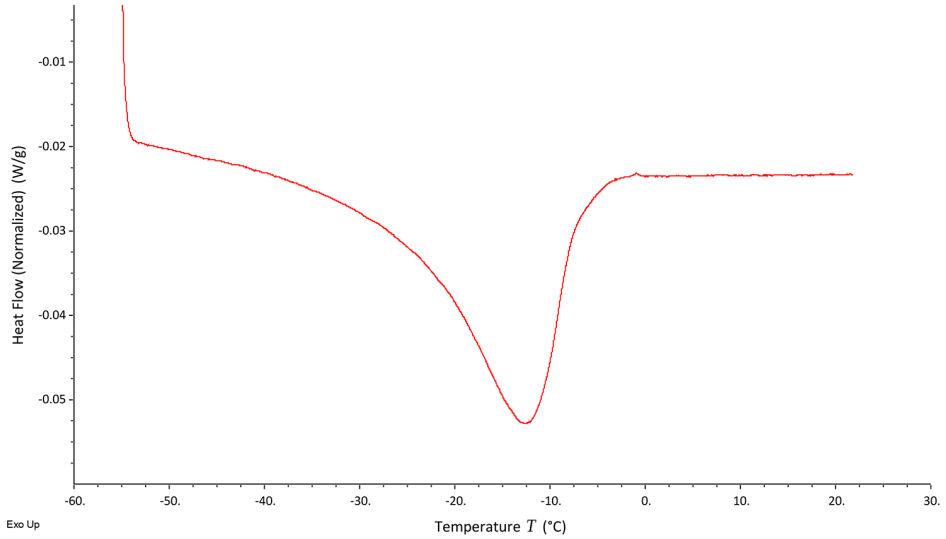

Figure 3.2: DSC melting curve for confined PdTA solution, $\phi = 0.355$, onset T_{melt} = -8.69 °C, peak T_{melt} = -12.65 °C. The total amount of liquid present in this sample is 0.179 mg based on a TGA measurement.

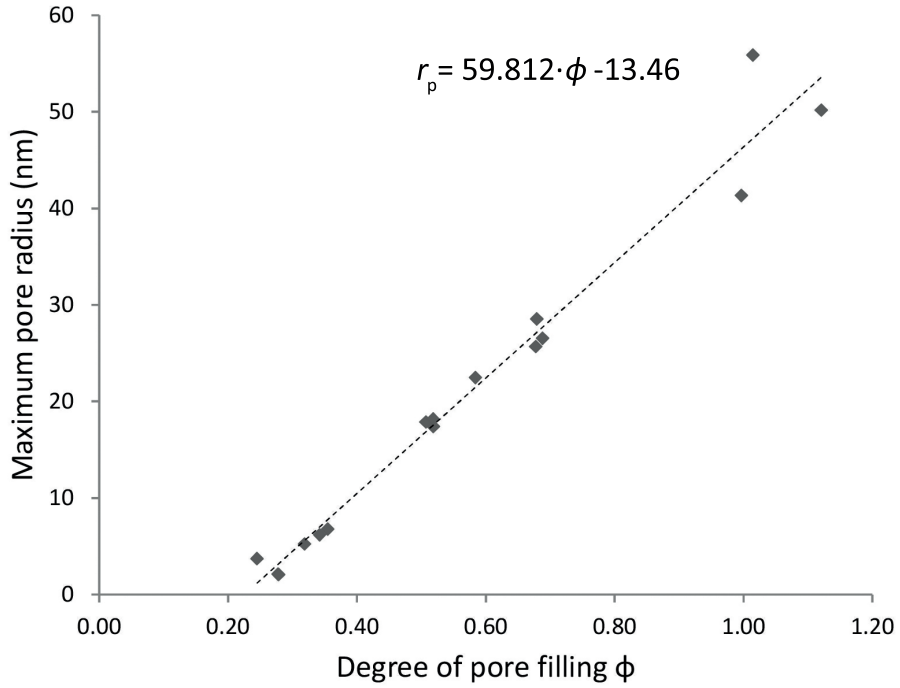

Figure 3.3: Correlation between degree of pore filling ϕ and the maximum pore radius of the filled pores r_{p} (in nm). Maximum pore radii calculated using Equation 3.5 with data from Table 3.1.

Melting behaviour in underfilled pores

Samples with underfilled pores ($\phi < 0.9$) showed a considerably smaller heat flow upon melting than samples with completely filled and overfilled pores, which is easily explained by the fact that a smaller amount of liquid is present in the pores. For samples with an extremely low loading ($\phi < 0.3$) the heat flow shows almost no change from the baseline in Figure 3.1, however as can be observed from Figure 3.2 a melting curve can still be obtained. This is because these samples contain only very little liquid. The radii for the pores that are filled in these low loadings were calculated to be between 2-4 nm, based on the onset melting temperature. This suggests that freezing barely takes place in these small pores, considering a non-freezing layer thickness δ of 0.8 nm. With a total pore diameter of 4 nm, only a radius of 1.6 nm of ice can be formed inside the pores. This corresponds to a thickness of around 11 molecules of frozen water based on the Lennard-Jones radius of a water molecule of 0.27 nm, which may explain the extremely low total enthalpy of melting observed for these samples.

An empirical linear relationship was obtained for the extent of impregnation and pore radius as depicted in Figure 3.3 by fitting a linear function to the dataset in Table 3.1. While this is a strictly empirical relationship which cannot be used to derive any physical data about the samples in question, it should be possible to predict the maximum pore radius filled for a given degree of pore filling, within a reasonable approximation.

Table 3.1: Melting temperatures of the PdTA solution in filled pores. The maximum filled pore radius r_p was calculated from the onset T_{melt}.

ϕ	onset T_{melt} (°C)	peak T_{melt} (°C)	r_p (nm)
0.245	−17.84	−16.69	3.72
0.278	−39.15	−19.48	2.13
0.278	−40.63	−22.29	2.08
0.319	−11.73	−15.31	5.23
0.342	−9.64	−13.30	6.19
0.355	−8.69	−12.65	6.78
0.507	−3.04	−8.25	14.88
0.518	−2.99	−5.14	18.18
0.519	−3.13	−5.62	17.41
0.584	−2.40	−3.60	22.49
0.678	−2.09	−3.00	25.69
0.679	−1.87	−2.68	28.55
0.688	−2.02	−2.87	26.54
0.997	−1.28	−2.08	41.33
1.015	−0.94	−2.01	55.88
1.121	−1.05	−2.22	50.18

3.4.3 Freezing behaviour of palladiumtetraamine in porous HSAG

Differential Scanning Calorimetry was also performed on the freezing process of the impregnated PdTA solution. As can be seen in Figure 3.4 the freezing and melting peaks are not present at the same temperature. Moreover, the freezing of pore water yields two peaks, where only one would be expected as a continuous distribution of pores is present in the sample. The freezing point depression can be attributed to the absence of nucleation sites for the pore water. Instead, the water is supercooled to such a point where all pore water freezes instantaneous. This can be better observed in Figure B.1. In this figure, the freezing thermograms for the samples in Table 3.1 are overlayed, displaying several steep inclines in the heat flow from the sample, resulting in a loop which is caused by the inability of the DSC apparatus to respond to the rapid change in heat flow. This was a larger issue for samples with a high degree of pore filling as opposed to those with a lower degree of pore filling (Figure 3.4). This can be fully attributed to the lower total amount of water to be frozen in samples with a lower degree of pore filling. This conclusion is supported by the fact that the onset of freezing of pore water is largely unrelated to the degree of pore filling.

3.4.4 Blocking of micropores and small mesopores

Toluene impregnation

Initially, an attempt was made to block the micropores using toluene (melting point: -95 °C, boiling point: 111 °C, solubility in water: 0.52 g/L at 20 °C) via dry impregnation as described in section 3.3.3 and subsequently impregnating the carbon with water to check whether pore blocking by toluene occurred. Water was used to simulate the PdTA solution as no difference in melting behaviour was observed between impregnations performed using a PdTA solution and the experiments performed by

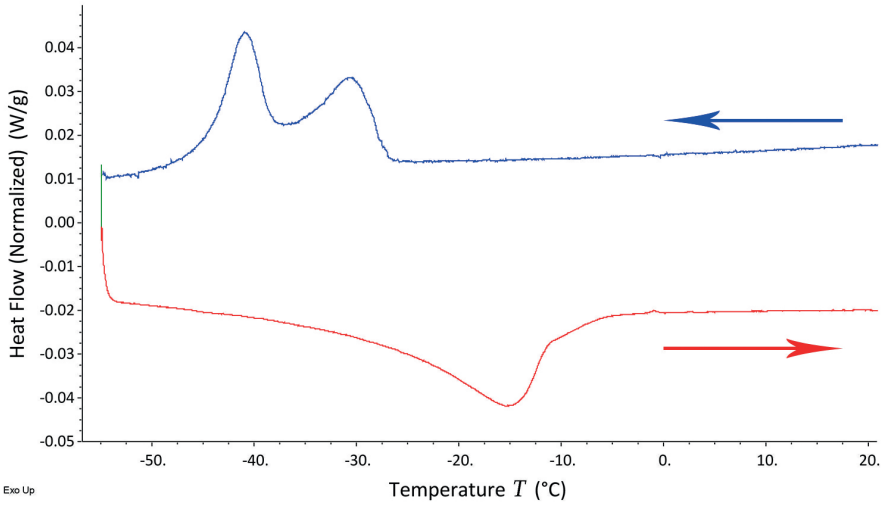

Figure 3.4: Discrepancy between melting- and freezing curves within a sample. The arrows indicate the scan direction of DSC. Note the two consecutive peaks in the freezing line (blue).

Den Brave[20]. Our theory for using toluene as a pore blocking agent was that toluene, as the first impregnant would first enter the micropores and would be held in place by capillary forces. After the toluene was added the water would only be able to impregnate the larger pores. The high boiling point of toluene would be beneficial in the synthesis of the final catalyst. This is because it may be possible that upon drying of the carbon the water from the PdTA solution would first evaporate, leaving the tetraamminepalladium precursor deposited in larger pores and toluene in the smaller pores. Only after evaporation of the water the higher-boiling toluene would evaporate, leaving the micropores and smaller mesopores completely empty.
The experimental conditions and results are summarized in Table 3.2, sample i-t-w. As can be seen, an amount of toluene representing a relatively large fraction of the pore volume (ϕ = 0.519) of the support was chosen, combined with a relatively small amount of water (ϕ = 0.282). It was thus expected that in the case of unsuccessful pore blockage, the peak melting temperature could be found at a temperature below -15 °C based on the results from Table 3.1. In the case of a successful pore-blocking experiment a peak melting temperature between -2 and -3 °C was expected, based on the the total pore-filling ϕ_{total} from Table 3.2 and the results from Table 3.1. However, the peak T_{melt} observed was near bulk at 0.153 °C. These results suggest that toluene could possibly form a film around the support particles, blocking access to the pores, thus preventing water from entering the support. However, this theory was not further explored.

Cyclohexanol impregnation

The results of pore blocking experiments using cyclohexanol as pore blocking agent can be found in Table 3.2. An initial experiment with impregnation of cyclohexanol (sample i-c) did not show any freezing- or melting peaks in DSC, which may indicate that freezing of the confined cyclohexanol may occur at temperatures outside of the instrument range, or even may not occur at all. Cyclohexanol impregnation with subsequent impregnation using water (i-c-w) gave a melting and freezing peak representative of a pore filling ϕ_{water} much higher than was impregnated in i-c-w.

Table 3.2: Summary of pore-blockage experiments. Experiment code is build up as follows: First letter stands for method of pore-blocking agent addition (i=impregnation, m=melt infiltration), second letter is the pore-blocking agent (t=toluene, c=cyclohexanol, p=phenol). Experiments ending with **w** were impregnated with water after impregnation with the pore-blocking agent. Repeat-experiments are numbered 1 through 3. Max. r_p was based on the formula found by plotting the degree of pore filling to the maximum filled pore radius in Figure 3.3. ϕ_{total} is the sum of the partial extent of pore filling using the pore blocking agent (ϕ_{PB}) and the extent of pore filling using water (ϕ_{PB}).

sample	ϕ_{PB}	ϕ_{water}	ϕ_{total}	onset T_{melt} (°C)	peak T_{melt} (°C)	max. r_p (nm)
i-t-w	0.52	0.28	0.80	0.32	0.15	34.5
i-c	0.19	-	0.19	-	-	-
i-c-w	0.18	0.17	0.35	-9.89	-12.75	7.5
m-p	0.17	-	0.17	-	-	-
m-p-w1	0.16	0.13	0.29	-19.91	-16.67	3.7
m-p-w2	0.21	0.20	0.41	-9.29	-5.77	11.2
m-p-w3	0.13	0.49	0.61	-0.92	-1.69	23.2
i-p	0.29	-	0.29	-	-	-
i-p-w	0.29	0.36	0.65	-3.11	-5.82	25.4

Taking ϕ_{total} as the maximum extent of pore filling where water may occur, the maximum pore radius filled with water was calculated to be 34.5 nm. As can be interpolated from Figure 3.3 and Table 3.1 the melting temperatures for i-c-w correspond to an extent of pore filling for water ϕ_{water} much closer to the value of ϕ_{total}. As cyclohexanol and water are not miscible to a large extent, an increase in melting point due to mixing was taken as unlikely. It was thus concluded that cyclohexanol is an effective pore blocking agent.
Unfortunately, cyclohexanol was difficult to accurately impregnate in the support. The melting point of cyclohexanol (25 °C) would in principle allow impregnation at elevated temperature. To this end, an amount of molten cyclohexanol was injected in the support-containing round-bottom flask using a syringe which was heated to a temperature well above 25 °C. Despite the elevated temperature, the cyclohexanol instantly solidified upon injection into the round-bottom flask with a part of the cyclohexanol being left in the syringe. This made it impossible to add cyclohexanol in a controlled fashion, which would make synthesis of a Pd/C catalyst employing a pore-blocking agent near impossible as it is not known beforehand how much of the pore blocking agent is inside the pores. Attempts to add solid cyclohexanol at room temperature to the support in order to perform a melt infiltration failed as well. The finely divided cyclohexanol would partially melt prior to addition making it impossible to accurately determine the amount of cyclohexanol added to the support.

Pore blockage by phenol melt-infiltration

Impregnation with liquid phenol at 50 °C using a syringe or glass pipette (samples (i-p, i-p-w, table 3.2) was attempted, but proved to be hard to handle for the same reasons outlined in the section on cyclohexanol impregnation. Also, it was found that addition at elevated temperature increased the likelihood of evaporation of the phenol after addition, instead of infiltration into the carbon pores.
Melt infiltration (samples m-p to m-p-w3) was studied as addition method, using the method described in section 3.3.5. This allowed for good control over the amount

of phenol added to the carbon support. Sample m-p, with only the addition of phenol, showed no freezing- or melting peaks in DSC over a temperature range from -70 °C to 50 °C. This is likely caused by a freezing point for nano-confined phenol of below -70 °C, which is outside of the measurement range, but was however not studied further. Experiments performed with melt-infiltration of phenol and subsequent impregnation with water, samples m-p-w to m-p-w3, showed similar results to impregnation using cyclohexanol. The increase in melting temperatures for pore water was not considered as caused by the mixing of phenol and water, as mixtures usually have a lower melting point than the pure substances and phenol only shows a low miscibility in water of 8.3 g phenol in 100 mL water.
The melting temperatures for the samples correspond to an extent of pore filling for water ϕ_{water} much closer to the value of ϕ_{total} as interpolated from Table 3.1. It was thus concluded that phenol is a good pore-blocking agent, as it can be added in a controlled manner and shows good pore blocking ability. The amounts of phenol infiltrated to calculate the extent of impregnation ϕ_{PB} in Table 3.2 were calculated with measurements from TGA, which is further explained in Appendix A.

3.5 Conclusions

A method to characterize the extent of impregnation for activated carbon using DSC and TGA was applied to a system containing high surface area graphite HSAG 500 and a palladiumtetraamine solution. The results from DSC and TGA were then used to calculate up to which pore radii were impregnated. It was found that a solution of tetraamminepalladium (II) nitrate could be impregnated into small pores by addition of small amounts of the solution. From DSC and TGA the maximum pore size containing the solution was then calculated.
Next, a method was developed to selectively impregnate larger mesopores in a micro- and mesoporous carbon using pore blocking agents. Small-pore blockage by toluene was unsuccessful which was probably caused by incompatibility of toluene with the support. Dry impregnation of hot cyclohexanol was successful, however it was not possible to accurately quantify how much was impregnated into the pores. Attempts for pore blockage by melt infiltration of cyclohexanol were unsuccessful. Phenol could reliably be infiltrated into the carbon support using melt infiltration. Melt infiltration of high surface area graphite (HSAG) using phenol and subsequent impregnation with water showed a shift towards higher temperature in the melting point of the confined water with respect to the amount of water impregnated on the untreated support, showing that pore water could be selectively impregnated into larger pores when smaller pores were blocked. It was thus concluded that melt infiltration with phenol can effectively be employed to block micro- and small mesopores of the carbon support.

Chapter 4

Catalyst synthesis and testing

4.1 Introduction

The aim of this project, as outlined in chapter 2, is to find the difference in activity and selectivity for the active metal catalyst particles confined in pores of different sizes. In order to study whether palladium crystallites formed in larger mesopores show a different activity and selectivity than crystallites formed in smaller mesopores and micropores, catalysts were prepared via the principles of selective impregnation outlined in the previous chapter. In theory, this could allow control over where in the porous support the tetraamminepalladium is deposited and thus where palladium crystallites are formed.

4.2 Theoretical considerations

4.2.1 Catalyst preparation

In the previous chapter, impregnation of the porous support was considered. In this chapter, we will discuss the remaining preparation steps.
After impregnation and homogenisation to distribute the solution evenly over the support grains, the support is dried at elevated temperatures under a gas flow. During drying,[12] most precursor molecules will lose the remaining NH_3 and NO_2 ligands and any metal precursor that had not adsorbed on the support surface will adsorb on the support surface as the liquid solution becomes saturated. Differences in heating rate and final temperature may cause a change in the particle size distribution, as the rate of evaporation of the water changes. This is even more important in the case of insufficient interactions between the surface and support, with the evaporating solvent carrying palladium to the outside of the pores.[8] This leads to egg-shell type distributions and a broad particle size distribution. It is therefore important that sufficient surface is properly functionalized in order for the metal to be linked to the support surface. Next, activation or reduction at elevated temperatures forms the final catalyst. The difference between activation and reduction is that in catalyst activation air or an inert gas such as N_2 is used, possibly obtaining oxidic nanoparticles while in reduction hydrogen gas is typically used as electron source, forming metallic nanoparticles. In this work however, electrons from the carbon support may be able to reduce the palladium to obtain metallic nanoparticles during activation under an N_2 atmosphere.

4.2.2 Hydrogenation using Pd/C catalysts

Palladium on carbon catalysts are widely used as hydrogenation catalysts, as mentioned in the first chapter. Cinnamaldehyde hydrogenation is often applied as a model hydrogenation reaction due to the fact that it is a small easy-to-handle α,β-unsaturated aldehyde. The coupled unsaturation gives three possible products[29] (Figure 4.1) from hydrogenation: the two partially hydrogenated products cinnamyl alcohol (**2**) and hydrocinnamaldehyde (**3**) and the fully hydrogenated hydrocinnamyl alcohol (**4**). This offers the ability to study the selectivity towards hydrogenation of different functional groups. Much research has been performed on controlling the catalyst selectivity in order to selectively hydrogenate the C=C bond to form hydrocinnamaldehyde (**3**). To this end several methods have been explored such as exchanging the carbon support for alumina or modifying the support used, the use of bimetallic catalysts and controlling the metal particle size.[30]
Research showed that control over selectivity can be gained by tuning the particle size[21,29,30]. It was shown that larger catalyst particles show higher selectivity towards the alcohol (**2**), while smaller particles show an increase in selectivity to the aldehyde (**3**). In addition, Nagpure[29] and Jiang[30] independently showed that formation of the fully hydrogenated product (**4**) exclusively occurs through hydrogenation of alcohol (**2**).
It was also suggested by Jiang[30] that the hydrocinnamaldehyde and cinnamyl alcohol are not interconverted by the catalyst, as the product distribution does not change after full consumption of cinnamaldehyde by the catalyst. They also showed that Pd/Al_2O_3 catalysts do not hydrogenate aliphatic aldehydes such as **3** by performing a hydrogenation reaction using a mixture of 1-hexene and hexaldehyde. After two hours reaction time, the *n*-hexene, solvent and hexaldehyde were found in the reaction mixture, without any hexanol present. It is thus suspected that the same will be true for Pd/C catalysts.
In the same paper, DFT calculations were used to study the cinnamaldehyde adsorption on the Pd surface to understand the particle size effect. As a model for a small

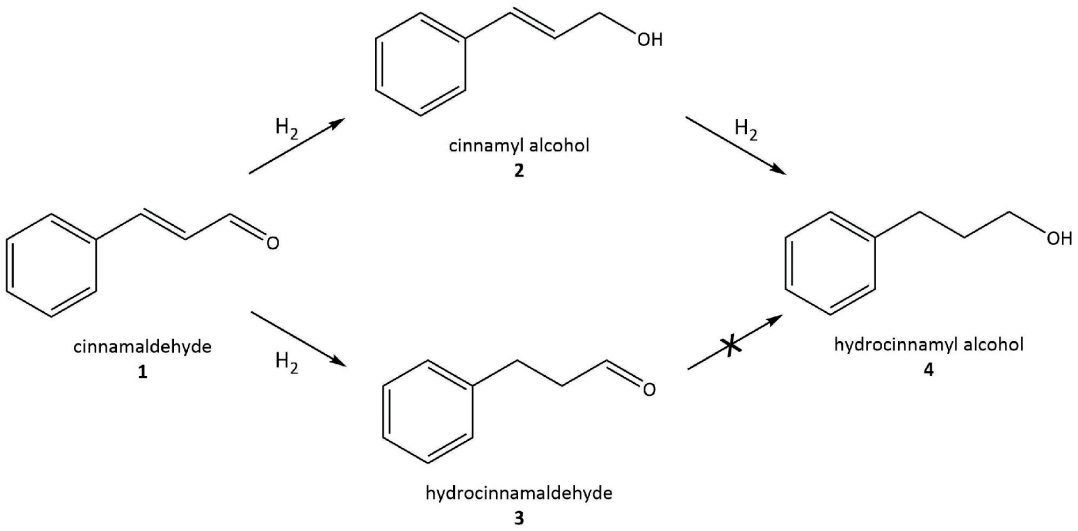

Figure 4.1: Hydrogenation of cinnamaldehyde using a Pd/C catalyst. Products cinnamyl alcohol **2** and hydrocinnamaldehyde **3** are obtained directly by hydrogenation of cinnamaldehyde, while hydrocinnamyl alcohol is only obtained via hydrogenation of cinnamyl alcohol **2** according to ref. [30].

Pd particle, the researchers used a Pd_4 nanocluster and for a large particle a slab model of Pd(111). Calculating the binding energy of C=C and C=O bonds on the two particle models, Jiang found that the C=C bond binds stronger on the nanocluster and weaker on the Pd(111) slab than the C=O bond. Stronger adsorption lead to an additional weakening of the π-bonds between the C=C and C=O bonds, leading to more facile hydrogenation of the bond in question. This means that the stronger binding of the C=C bond to the Pd_4 nanocluster lead to a higher selectivity towards hydrocinnamaldehyde formation. In the reverse, the stronger C=O bond adsorption on the Pd(111) slab with respect to binding of the C=C bond to the Pd(111) slab lead to a higher selectivity towards cinnamyl alcohol formation.

4.3 Experimental procedure

4.3.1 Materials

Activated carbon GSX (steam activated, acid washed), biphenyl (99%) was obtained from Norit and tetraammine palladium (II) nitrate (PdTA) solution, (51.9 mg Pd/mL solution) was acquired from Alfa Aesar. Trans-cinnamaldehyde (99%) and phenol (99%, extra pure) were obtained from Acros Organics. 2-Propanol (puriss., ≥99.5% (GC)) was obtained from Sigma-Aldrich. In all experiments MilliQ demineralized water was used, unless stated otherwise.

4.3.2 Support functionalization

Activated carbon was functionalized by refluxing in 10% HNO_3 for 30 minutes at a heating mantle temperature set to 170 °C. After refluxing, the reaction was allowed to cool to room termperature and subsequently filtered and washed 6 times with demineralized water using a Büchner funnel to remove any HNO_3 remaining. The functionalized carbon was then dried overnight in a stove at 60 °C as the hygroscopic carbon did not need to be completely dry at this point. This resulted for Norit GSX activated carbon in an acid functional group density of 0.2 nm^{-2} as determined using equation 4.1.

4.3.3 Surface acid group concentration determination

The concentration of acid groups on the carbon support was calculated from the BET surface area obtained from N_2 physisorption and base titration using a Titralab TIM 880. Using a 0.01 mol/L sodium hydroxide solution as titrant, a curve was obtained for the pH increase against volume of titrant added. The first derivate was calculated for this curve to obtain the exact inflection point, fitting the curve obtained using a polynomial function. From this, the surface density of acid groups can be calculated via the formula:

$$\rho_{\text{Acid sites}}(nm^{-2}) \;=\; \frac{0.01\ (mol \cdot L^{-1}) \cdot V_{\text{IP}}\ (L)\ \cdot N_{\text{A}}\ \cdot 10^{-18}}{A_{\text{BET}}\ (m^2) \cdot m_{\text{s}}\ (g)} \tag{4.1}$$

With V_{IP} the volume of NaOH solution added at the inflection point represented by the maximum in the curve, N_{A} the Avogadro constant, A_{BET} the BET surface area and m_{s} the sample mass. The surface density of acid groups $\rho_{\text{Acid sites}}$ is then given in units of nm^{-2}.

4.3.4 Catalyst preparation

Catalysts were prepared by first weighing 0.3 grams of the functionalized support in a 250 mL round-bottom flask equipped with septum, valve and magnetic stirrer. Next, the carbon was dried at 170 °C under vacuum using an electric heating mantle and vacuum pump. After two hours, the heating mantle was removed and the round-bottom flask valve was closed to create a static vacuum. When the flask was cooled to room temperature, the aqueous PdTA solution was added under vacuum using a syringe. In the case of selective impregnation of the precursor into the larger mesopores (catalysts **c03-03L** and **c07-02L**, Table 4.1), the smaller mesopores and micropores were first blocked with phenol using melt infiltration. To this end, the vacuum was first removed by filling the round-bottom flask with N_2 through the valve using a balloon. The solid phenol was then added by first removing the valve. The valve was then replaced on the round bottom flask within seconds to prevent water-vapour containing air to enter the flask. The PdTA solution was then added through the septum using a syringe to prevent unnecessary exposure to air. Sample **c0-10L** was prepared by first diluting the PdTA solution with water, using a ratio of 2.9:1 water to PdTA solution by weight.
After impregnation of the carbon support with the Pd-precursor solution, the sample was dried and reduced in a glass reactor using a fluidized bed configuration under a nitrogen flow of 100 mL per minute. Drying was performed at 100 °C for 2 hours with subsequent activation at 500 °C for 2 hours with a temperature ramp of 5 °C/min between the isothermal sections. In Table 4.1, the prepared catalysts for testing are summarized.

Table 4.1: Catalysts prepared for catalytic testing. ϕ_{phenol} and ϕ_{PdTA} indicate the degree of pore filling with phenol and the PdTA solution respectively. The palladium loading is given in the last column as a measure of weight-% of the weight of the support and was calculated from the amount of PdTA solution impregnated.

catalyst	ϕ_{phenol}	ϕ_{PdTA}	ϕ_{total}	Pd loading (wt.%)
c0-10L	-	1.01	1.01	1.33
c0-10H	-	1.05	1.05	4.93
c0-03L	-	0.29	0.29	1.52
c0-06H	-	0.68	0.68	3.93
c03-03L	0.34	0.30	0.64	1.61
c07-02L	0.65	0.24	0.89	1.30

4.3.5 Catalyst testing

Catalyst testing was performed using an autoclave set-up from Autoclave Engineers, depicted as a schematic in Figure 4.2, equipped with a mechanical stirrer. In a typical experiment, the reactor was filled with 25 mg of catalyst, together with 60 mL of 2-propanol as solvent. A cinnamaldehyde solution was prepared for each catalytic test. This solution was made in a 50 mL volumetric flask and consists of 108 mg biphenyl as internal standard, together with 2.64 g trans-cinnamaldehyde. 2.5 g demineralized water was added to prevent acetal formation. The flask was filled to total 50 mL using 2-propanol. Of this solution, 30 mL was loaded into the charge vessel.
The reactor and charge vessel were heated to 60 °C and stirring set to 400 rpm. After

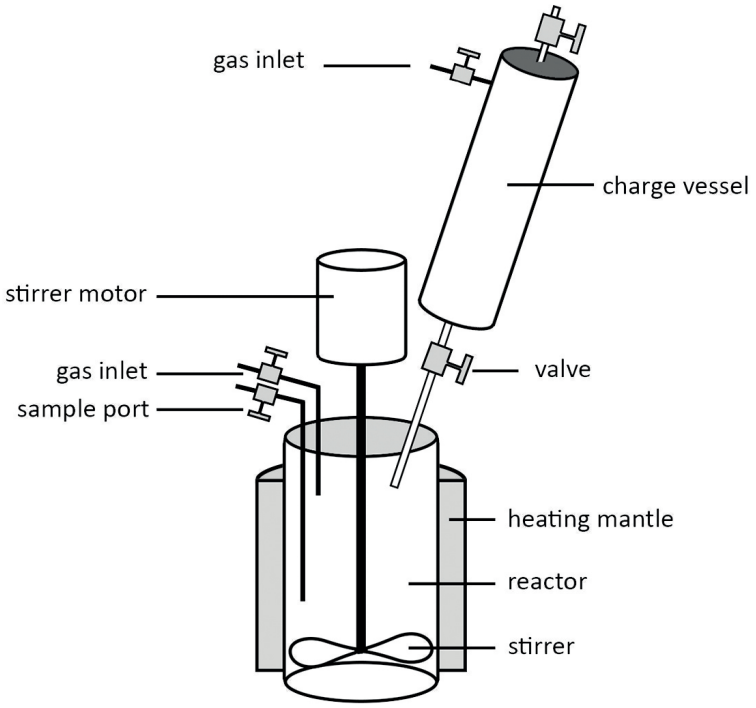

Figure 4.2: Basic schematic of autoclave setup. Note that the stirrer depicted is not the type of stirrer used. The reactor is first filled with the catalyst and isopropanol, heated to 60 °C and pressurized to 15 bar with H_2. The reaction is then started when the cinnamaldehyde solution in the charge vessel (pressurized to 25 bar with H_2) is released to the reactor.

allowing the reactor temperature to stabilize for 20 minutes, the reactor was pressurized using hydrogen gas to 15 bar. Once pressurized, the hydrogen gas flow was switched to the charge vessel, which was pressurized to 25 bar. The hydrogenation reaction was then started by opening the valve between the chargevessel and reactor, forcing the reactants in the charge vessel into the reactor setting the hydrogen gas pressure at 20 bar. The final amounts of cinnamaldehyde, catalyst and water present in the reactor is given in Table 4.2.
After the reaction was started, samples were taken from the reactor at set intervals, flushing the sampling tube with 0.5 mL from the reaction mixture before collecting the sample. Samples taken were between 0.5 and 1 mL in size.

Table 4.2: Amounts of cinnamaldehyde, catalyst, palladium and water present in the reactor during catalytic testing. The amount of palladium present in the reactor was calculated from the amount of catalyst in the reactor and the palladium weight loading of the catalyst in question.

catalyst	cinnamaldehyde (mol/L)	catalyst (mg)	Pd (mg)	water (g)
c0-10L	0.100	25.96	0.35	1.49
c0-10H	0.103	25.03	1.23	1.49
c0-03L	0.101	26.23	0.40	1.51
c0-06H	0.100	29.02	1.14	1.50
c03-03L	0.100	25.76	0.41	1.50
c07-02L	0.100	25.43	0.33	1.50

4.3.6 Characterization methods

N_2 physisorption measurements were performed using a Micromeritics Tristar 3000. To calculate the total surface area, the BET method was applied. To obtain a bulk Pd-crystallite size, X-ray diffraction (XRD) was performed on a Bruker D2 Phaser powder X-ray diffractometer using Co K_α radiation (λ = 1.79026 Å). Measurements were carried out from 40-90° 2θ. High Angle Annular Dark Field Scanning Transmission Electron Microscopy (HAADF-STEM) images were recorded on a FEI Talos F200X transmission electron microscope. iTEM and ImageJ software packages were used to measure the size of palladium particles for hundreds of particles per sample. H_2 chemisorption was measured on a Micromeritics ASAP 2020C. Samples taken during catalytic testing were analysed using a Shimadzu GC-2010 equipped with a flame ionization detector.

4.4 Results and discussion

4.4.1 Catalyst characterization

Catalysts **c0-10L** and **c0-10H** (Table 4.1) were prepared by full impregnation, with different palladium loadings on the support. The catalyst with lower weight loading **c0-10L**, had a mean Pd-particle size of 3.78 $\pm$ 1.20 nm as calculated from STEM images, while the catalyst with higher Pd-weight loading **c0-10H**, had a mean Pd-particle size of 4.69 $\pm$ 1.75 nm as can be seen in Table 4.3. This result was expected as a higher amount of palladium on the same surface area is likely to result in a larger particle size. STEM images of **c0-10L** (Figure 4.3a) reveal relatively small particles with large empty sections, caused by the low palladium loading on the carbon. These empty areas were not observed for **c0-10H** (Figure 4.3b).
Catalyst **c03-03L** has a similar Pd loading as **c0-10L**, with the major difference that **c03-03L** was prepared by melt infiltration with phenol up to $\phi = 0.34$ and subsequent impregnation using the PdTA solution ($\phi = 0.30$). This resulted in a mean Pd particle size of 5.70 $\pm$ 1.72 nm as determined from STEM. This means that at a comparable weight loading, the mean particle size has increased from 3.78 $\pm$ 1.20 nm to 5.70 $\pm$ 1.72 nm upon pore blockage by phenol prior to impregnation with the PdTA precursor. In Figure 4.3f, the same open spaces that were present in **c0-10L** can be seen for **c03-03L**. However, the large Pd particles of 10 nm and above observed in **c03-03L** were not previously seen. It seems that this may be either due to particles having more room to grow as they are not confined in smaller pores which do not allow for such growth or due to blockage of the smaller pores and thus less available support surface for palladium deposition when the catalyst was dried. It is however important to note that while in **c0-10L** the pores were completely filled at $\phi_{\text{total}} = 1.01$, in **c03-03L** the pores were underfilled at $\phi_{\text{total}} = 0.64$. This makes it less plausible that not enough surface area was available on the support for small particles to be present.
Comparing the results, it would be expected that for **c0-03L** relatively small particles would be observed as compared to **c0-03L** due to low palladium loading, combined with the small impregnation volume. This would mean that for **c0-06H** slightly larger particles would be obtained than for **c0-03L**, as the weight loading is much higher (as well as the higher pore filling of $\phi_{\text{total}} = 0.29$ for **c0-03L** versus $\phi_{\text{total}} = 0.67$ for **c0-06H**). However, the particle size obtained for **c0-03L** and **c0-06H** were nearly equal with 5.25 $\pm$ 1.98 nm and 4.87 $\pm$ 2.34 nm respectively. In Figure 4.3c,d, TEM images for **c0-03L** can be seen. It was noticed that some support particles contained

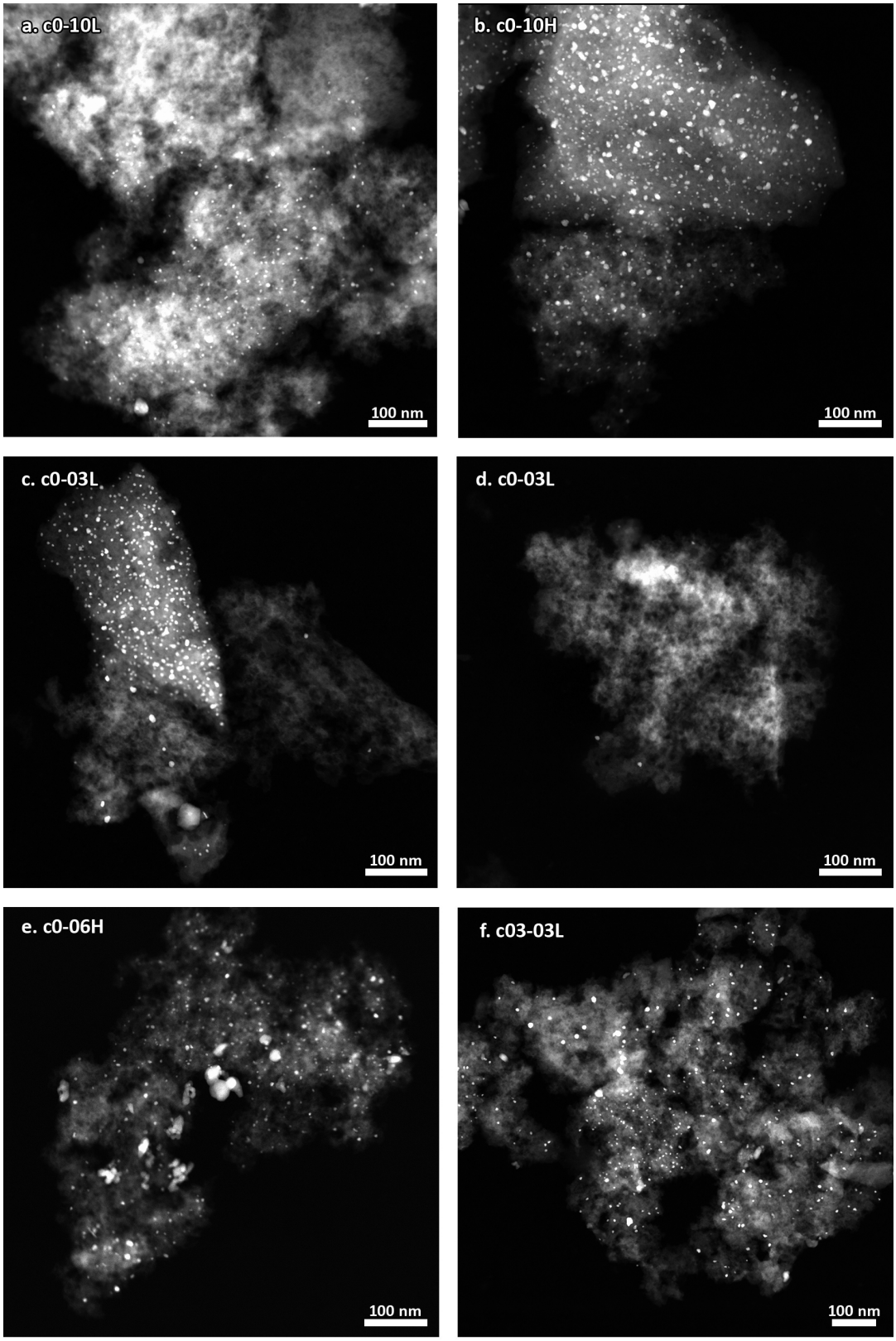

Figure 4.3: Summary of STEM images from **a**. catalyst c0-10L **b**. catalyst c0-10H **c**,**d**. catalyst c0-03L **e**. catalyst c0-06H and **f**. catalyst c03-03L

almost no metal particles, while in some catalyst grains relatively high densities of particles were obtained. Again, this could be explained by the low impregnation volume with a more concentrated PdTA solution. It should not come as a surprise then that for **c0-06H** (Figure 4.3e), a higher concentration of palladium particles can be found, with a similar palladium particle size as **c0-03L**. As can be seen in Figure 4.4, the palladium particle size distribution shows a very similar size distribution for palladium particles in catalysts **c0-03L** and **c0-06H**, with a small fraction of particles in catalyst **c0-06H** being larger than 14 nm. Note however that large aggregates as can be seen in Figure 4.3 were not taken into account in the particle size distributions when a clear border could not be defined, which may change this picture somewhat. These results suggest that the particle size is an effect of the concentration of the precursor in the impregnation solution used and that partial impregnation combined with or without pore blockage by phenol has only a small effect on the particle size. In Table 4.3, the crystallite size obtained from XRD measurements can be found as obtained for the Pd(111) plain, which all show an average Pd crystallite size between 4 and 5 nm. As the crystallite sizes denoted here are the average crystallite size, the results obtained from XRD may not be a good measure for the palladium particle size distribution, even more so as results from STEM show a different picture than XRD.
In the same table, the surface area of palladium in the catalysts can be found. These are given in surface area per gram of catalyst. It is interesting to see that the metallic surface area of catalyst **c0-03L** is higher than that of **c03-03L** at nearly equal palladium loading and particle size. This seems to be an effect of the phenol added in **c03-03L**. A possible explanation is that more palladium aggregates are present in **c03-03L** than in **c0-03L**, which can significantly reduce the palladium surface area. Else, a possibility is that phenol is adsorbed on the palladium surface during catalyst preparation, blocking the palladium surface.

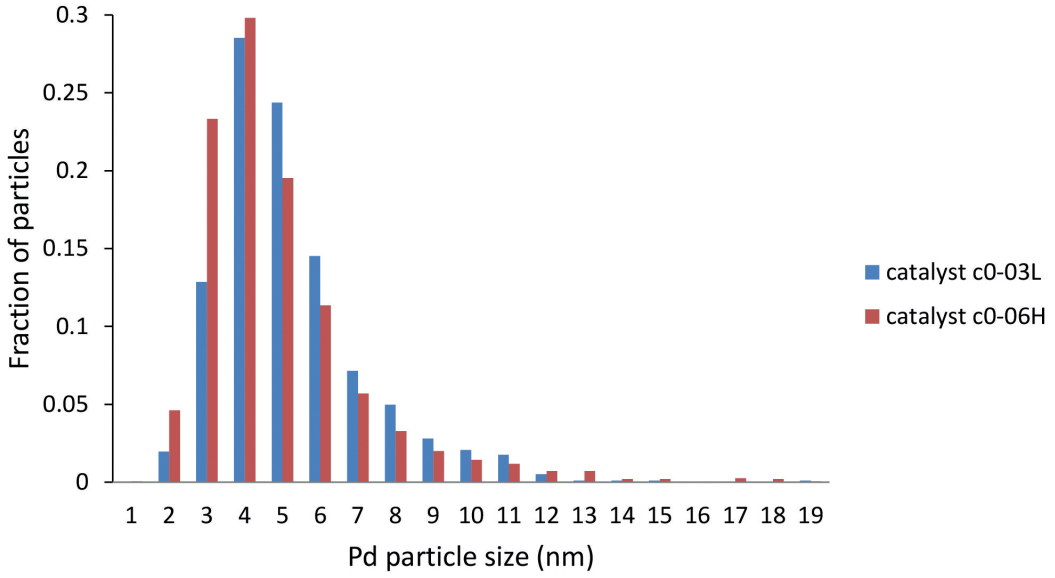

Figure 4.4: Palladium particle size distribution for catalysts c0-03L and c0-06H. The denoted particle size is in the range $\pm$ 0.5 nm.

Table 4.3: Average Pd particle size obtained from STEM for both fresh and spent catalysts. Also, the crystallite size was determined using XRD and the metallic surface area (in m^2 per gram of catalyst) was measured using H_2 chemisorption.

catalyst	particle size (nm)	particle size (spent) (nm)	crystallite size (nm)	surface area (m^2)
c0-10L	3.78 ± 1.20	3.57 ± 1.60	4.40	-
c0.0-1.0H	4.69 ± 1.75	4.56 ± 1.88	4.06	2.61
c0.0-0.3L	5.25 ± 1.98	3.09 ± 1.88	4.97	1.03
c0.0-0.6H	4.87 ± 2.34	-	4.44	-
c0.3-0.3L	5.70 ± 1.72	5.69 ± 2.15	4.43	0.64
c0.7-0.2L	-	-	4.00	-

Spent catalysts

Several spent catalysts were imaged using STEM. No significant increase in particle size was found, as can be seen in Table 4.3. One deviation is apparant: For **c0-03L**, a decrease in particle size can be seen. In Figure 4.5 this discrepancy is further expanded. What can be seen is that the spent catalyst has a lot of particles between 1 and 3 nm in diameter, while the fresh catalyst has more particles between 3 and 6 nm in diameter. No apparent reason can be found for this decrease in particle size. The STEM images of the spent catalysts can be found in Appendix C and particle size distribution plots for the remaining catalysts can be found in Appendix D. These distributions show no apparent difference can be found between the fresh and spent catalysts for the particle size distributions of catalysts **c0-10L**, **c0-10H** and **c03-03L**

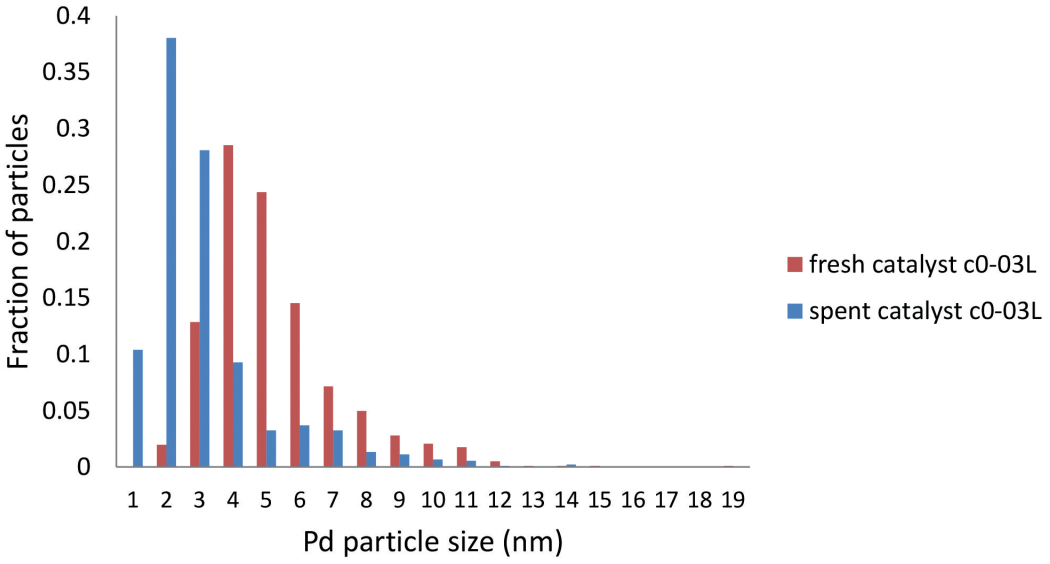

Figure 4.5: Comparison between the particle size distribution of fresh and spent catalyst c0-03L. The denoted particle size is in the range $\pm$ 0.5 nm.

4.4.2 Catalyst testing

Conversion of cinnamaldehyde

The prepared catalysts were tested for the catalytic hydrogenation of cinnamaldehyde. In figure 4.6 the conversion of cinnamaldehyde by the different catalysts is summarized. What can immediately be seen is that after approximately 180 minutes the conversion of cinnamaldehyde was completed for the fully impregnated catalysts **c0-10L** and **c0-10H**. As both catalysts **c0-10L** and **c0-10H** follow the same path for conversion it can be concluded that increasing the Pd loading of the catalysts beyond that of **c0-10L**, which has a Pd weight loading of 1,33%, does not increase the conversion of cinnamaldehyde by a significant amount. This is because at every point during the catalytic reaction, nearly the same amount of cinnamaldehyde is present in the reactor. In **c0-10L** only 0.35 mg of palladium is present in the reactor, while in **c0-10H** 1.23 mg palladium is present in the reactor as can be seen in Table 4.2.
Catalyst **c0-03L** followed a similar cinnamaldehyde conversion path, which is interesting as this catalyst has a similar loading as **c0-10L**, but it was prepared by partial impregnation of the support. Based on these results, it may be expected that the catalytically active palladium may be present in similar locations for catalysts **c0-03L** and **c0-06H**. Catalyst **c0-06H** showed an intermediate conversion. In first instance, it was thought that this has less to do with the catalyst itself and that experimentally something must have gone wrong as the similar catalyst **c0-03L** did show full conversion of cinnamaldehyde. It was however confirmed that the autoclave performed as normal during the catalytic reaction, not showing any decrease in H_2 pressure, temperature or stirrer speed. Catalyst **c03-03L** and **c07-02L**, prepared by melt infiltration with phenol and subsequent impregnation using the PdTA solution, only achieved a low conversion of 15.5% and 21% respectively, making these the worst-performing catalysts tested. A possible explanation could be that relatively large particles present in large pores perform worse in this catalytic hydrogenation. This would be quite surprising, as these large pores should be more accessible than the small pores.
These results suggest that smaller palladium particles trapped in smaller pores exhibit a higher catalytic activity than the larger particles in the large mesopores.

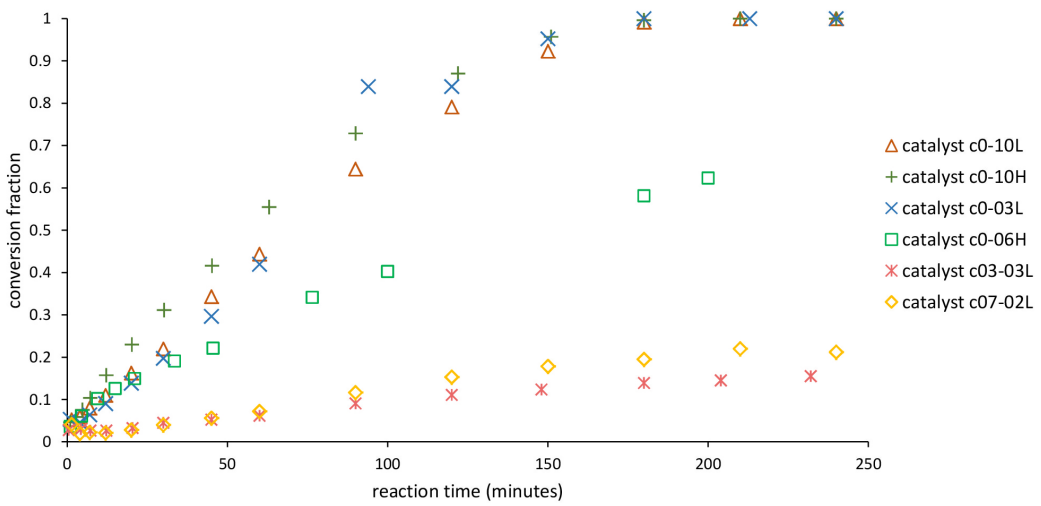

Figure 4.6: Conversion of cinnamaldehyde. After 180 minutes the reactions seemed completed as no significant conversion took place after that time.

Reaction rate

In order to obtain insight into the kinetics of the hydrogenation reaction to explain the obtained results, the initial reaction rate was calculated, see Table 4.4. The rate was calculated from the amount of cinnamaldehyde that was hydrogenated over the first four minutes of hydrogenation, the results in the table thus reflect the average initial rate per second over the first four minutes. An earlier sampling point could be taken for the calculation, but some variability was found in the cinnamaldehyde concentration due to insufficient mixing of all reagents after one minute of reaction time. The initial reaction rates are normalized to the amount of palladium present (second column) and to the adsorption sites present on the catalyst as determined by H_2 chemisorption, giving the turnover frequency. It is here important to note that the adsorption sites are defined as one site per surface palladium atom. Computational studies performed by Jiang[30] however show there are two different adsorption sites, dependent of the bond being hydrogenated. C=O bond adsorption on nanoclusters indeed showed a single adsorption site per palladium atom, however C=C bond adsorption on the flat Pd(111) surface was calculated to involve two palladium atoms. This two-atom adsorption site was not taken into consideration into the calculations, instead a single palladium atom was taken as the average adsorption site.
As can be seen in the first column, a high initial rate per gram Pd can be found for **c0-10L**, as well as a slightly lower rate for **c0-03L**, which can be explained by the low Pd loading of these catalysts (Table 4.1). **c0-03L** has slightly larger particles than **c0-10L** which is reflected in the slightly lower rate. Catalysts **c0-10H**, **c0-06H**, **c03-03L** and **c07-02L** all have a similar initial rate. The relatively low initial rates of **c0-06H**, **c03-03L** and **c07-02L** correlate with the fact that only a small part of the cinnamaldehyde is hydrogenated. However, **c0-10H** shows an almost equal initial reaction rate to **c0-06H**. This could be explained by a low surface-to-bulk ratio of palladium due to the high Pd loading, with less on surface palladium to perform the hydrogenation reaction.
In Table 4.4 the TOF is given for three reactions. Catalysts **c03-03L** shows a slightly lower TOF than **c0-03L**, but much a much higher TOF than **c0-10H** which is interesting as the reactions for **c0-03L** and **c0-10H** give full cinnamaldehyde conversion and the reaction for **c03-03L** does not. This means that catalyst deactivation of **c03-03L** has not occurred during catalyst preparation. Both catalyst **c0-03L** and **c03-03L** do

Table 4.4: Initial reaction rate and turnover frequency (TOF), determined as an average per second over the first four minutes of reaction time. The initial rate was normalized per gram of palladium present in the reactor (calculated from the total amount of catalyst added to the reactor) and for the TOF per adsorption site in the reactor, as calculated from H_2 chemisorption measurements. For reference, the palladium particle size of the spent catalysts from Table 4.3 is added in the last column.

catalyst	initial rate mol s^{-1} (g Pd)$^{-1}$	TOF (s^{-1})	Pd particle size (spent) (nm)
c0-10L	0.00778	-	3.57 ± 1.60
c0-10H	0.00294	3.20	4.56 ± 1.88
c0-03L	0.00576	4.72	3.09 ± 1.88
c0-06H	0.00239	-	-
c03-03L	0.00345	4.24	5.69 ± 2.15
c07-02L	0.00302	-	-

however have a practically identical palladium loading as can be seen in Table 4.1. It therefore seems reasonable to suggest that the catalyst becomes deactivated during the cinnamaldehyde hydrogenation reaction. It was already commented on that the low initial rate of **c0-10H** was due to a low surface to bulk palladium ratio. This seems to hold true for the TOF as well when comparing catalysts **c0-10H** and **c0-03L**. One possibility for the incomplete hydrogenation of cinnamaldehyde using catalysts **c03-03L** and **c07-02L** is due to Ostwald ripening of the palladium particles. This process causes a decrease in total surface area as more of the palladium goes to the bulk of the particles. This is however not consistent with the results displayed in Table 4.3. It would also offer an explanation for the selectivity observed in Figure 4.7e,f: in Ostwald ripening the size of smaller particles decreases in favour of an increase in the size of the bigger particles, enabling an increase in the rate of hydrocinnamaldehyde formation as the palladium particles become smaller. Formation of hydrocinnamaldehyde would slow down as the smaller particles are depleted, which is an effect that cannot be ruled out by the graphs in Figure 4.7e,f. This Ostwald ripening process could be enabled by the fact that the small mesopores and micropores were blocked during catalyst preparation causing palladium particles to exclusively form in larger meso- and macropores. Unfortunately, this conclusion is not backed up by the TEM images (Figure 4.3 and Appendix C) and particle size distributions (Appendix D) obtained from the fresh and spent catalyst **c03-03L** though it is possible, however unlikely, that a large bulk of palladium was missed in the observations made of spent **c03-03L**.
Another possibility is that phenol, used during catalyst preparation, is adsorbed on the palladium nanoparticles. This would deactivate the catalyst, preventing the hydrogenation of cinnamaldehyde. While this would explain the low conversion of cinnamaldehyde, the high TOF of **c03-03L** seems to contradict this explanation. If deactivation by adsorption of phenol does play a role, it would seem that it is a contributing factor in catalyst deactivation, but is not the only reason for catalyst deactivation to occur.

Catalyst selectivity

In Table 4.5 the product distribution after a reaction time of 180 minutes is given. 180 minutes was chosen as a good time for comparison, because in catalysts **c0-10L** and **c0-10H** nearly all cinnamaldehyde had just been hydrogenated and the product distribution did not shift much after this time. In the second column of Table 4.5, the remaining amount of cinnamaldehyde is given as reference. It is noticeable that that the two fully impregnated catalysts **c0-10L** and **c0-10H** show a similar product

Table 4.5: Product distribution at 180 minutes reaction time. CALD = trans-cinnamaldehyde, CALC = cinnamyl alcohol, HALD = hydrocinnamylaldehyde, HALC = hydrocinnamyl alcohol.

catalyst	CALD (mol%)	CALC (mol%)	HALD (mol%)	HALC (mol%)
c0-10L	0.82	0.54	23.8	74.9
c0-10H	0.37	1.17	12.7	85.8
c0-03L	0	0	35.0	65.0
c0-06H	41.9	2.89	46.1	9.13
c03-03L	86.1	2.67	8.17	3.08
c07-02L	80.5	4.15	8.86	6.49

distribution after 180 minutes with the difference between them that **c0-10L** has a hydrocinnamaldehyde to hydrocinnamyl alcohol ratio of 1:3.15 and **c0-10H** a ratio of 1:6.76. Also, **c0-10H** contains slightly more cinnamyl alcohol.

As explained in section 4.2, larger particles lead to a higher degree of cinnamyl alcohol formation. In Figure 4.7a,b conversion of cinnamaldehyde into the products are followed over time for **c0-10L** and **c0-10H**. What can be seen is an increase in cinnamyl alcohol in the first hour of the reaction, with subsequent decay as cinnamyl alcohol is further hydrogenated to hydrocinnamyl alcohol. In both reactions hydrocinnamyl alcohol is formed in large quantities (and thus cinnamyl alcohol also has to be formed in large quantities). In Figure 4.7a,b a difference can be seen in the maximum of cinnamyl alcohol production between **c0-10L** and **c0-10H** at 60 minutes reaction time. This shows that less cinnamyl alcohol (molfraction of 0.06) is formed over the reaction duration by **c0-10L** than by **c0-10H**, reaching a molfraction of 0.13 for cinnamyl alcohol, resulting in a higher fraction of hydrocinnamyl alcohol in the final product distribution of **c0-10H** than in that of **c0-10L**. This is most likely due to the larger palladium particles present in **c0-10H**, as compared to **c0-10L**.

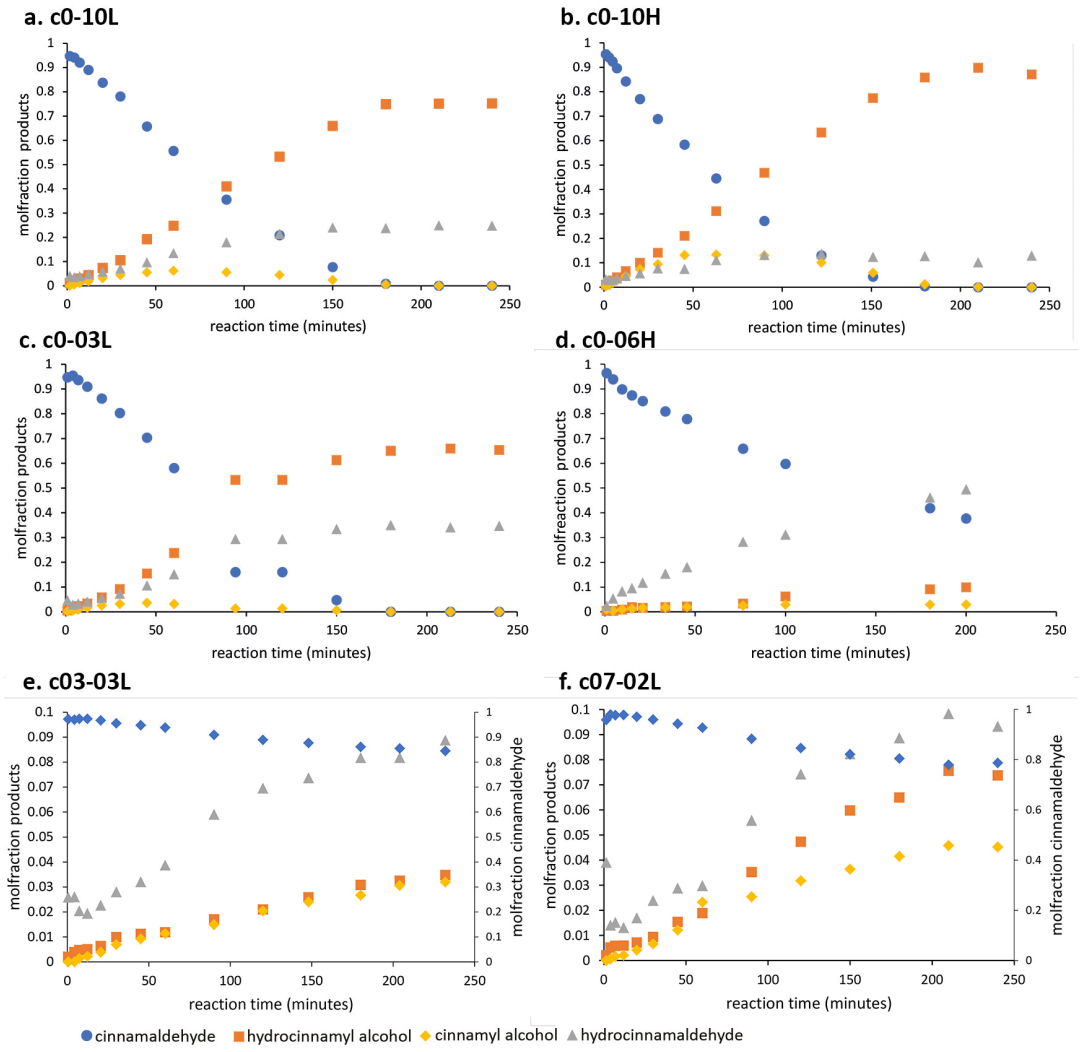

Figure 4.7: Conversion of cinnamaldehyde into the hydrogenation products followed over time for catalyst **c0-10L** (**a**) and catalyst **c0-10H** (**b**).

Catalytic tests for **c0-03L** and **c0-06H**, prepared by partial impregnation of the support with the palladium precursor, were followed over time and the results can be found in Figure 4.7c,d. It is interesting to see that while **c0-03L**, just as **c0-10L** and **c0-10H**, reached full conversion of cinnamaldehyde a relatively large amount of hydrocinnamaldehyde is formed in **c0-03L** compared to **c0-10L** and **c0-10H**.
This increase in hydrocinnamaldehyde formation in **c0-03L** may be an effect of the palladium particles possibly being present in the small pores. While smaller particles were counted for **c0-10L** than for **c0-03L**, the spent catalyst **c0-03L** contained numerous small particles of between 1 and 3 nm in diameter, as can be seen in Figure 4.5. Apparently, the average palladium particle size has decreased in this catalyst, contributing to the large amount of hydrocinnamaldehyde being formed.
This does not explain why **c0-06H** has a relatively low conversion combined with an even higher hydrocinnamaldehyde selectivity than in **c0-03L**. As was commented on before, **c0-06H** was prepared with a higher degree of pore filling and higher overall loading. Taking results from the previous catalysts into consideration, a complete conversion of cinnamaldehyde was expected. It is however interesting to see that this catalyst performed best for the formation of hydrocinnamaldehyde. This seems to exclude experimental error as the cause for the low conversion. On the other hand, palladium particles in **c0-06H** are larger than those found in **c0-03L**. This would suggest that **c0-06H** should produce less hydrocinnamyl aldehyde than **c0-03L**. A possibility could be that the palladium particle size decreased significantly during catalysis in **c0-06H**. If shrinking of enough particles were to continue, it could also explain the low conversion of cinnamaldehyde observed, as not enough surface area is available for cinnamaldehyde hydrogenation to complete within the experiment duration. Unfortunately, STEM images are not available for this spent catalyst and this reasoning cannot be confirmed.
As conversion of cinnamaldehyde was very poor for the catalysts prepared by melt infiltration with phenol with subsequent PdTA-solution impregnation, the conversion of cinnamaldehyde was was put on the secondary y-axis in Figure 4.7e,f, with the hydrogenation products on the primary y-axis. It is relatively noticeable that an excess of hydrocinnamaldehyde is present in both **c03-03L** and **c07-02L**. This would not be expected as the large particles present in the large mesopores and macropores would favor formation of cinnamyl alcohol. However, hydrocinnamyl alcohol is only formed through the hydrogenation of cinnamyl alcohol as mentioned in section 4.2.2. Combining the share of cinnamyl alcohol and hydrocinnamyl alcohol in experiment **c07-02L**, a combined yield of 11.9 mol% is obtained for cinnamyl alcohol and hydrocinnamyl alcohol. This is slighly higher than the yield obtained for hydrocinnamaldehyde (9.32 mol%), as is expected for the larger particles. It is however unclear why not all cinnamyl alcohol is hydrogenated to hydrocinnamyl alcohol by this catalyst.

4.5 Conclusions

Particle size distributions showed more larger particles observed for catalysts prepared with a high palladium weight loading. It was notable that palladium particle growth did not occur during catalysis, as observed from the spent catalysts. More large palladium particles were present on the spent catalysts, however this did not affect the average particle size by a large amount. In the case of a catalyst prepared by partial impregnation at low palladium loading, a decrease in particle size could be observed for the spent catalyst. Activity and selectivity were as expected for the catalysts prepared by full impregnation, both at high and low palladium loading on the catalysts. As expected, it was found that a catalyst with larger palladium particles resulted in more cinnamyl alcohol (and thus subsequently more hydrocinnamyl alcohol) formation, and smaller particles resulted in an increase in hydrocinnamaldehyde formation. The same relationship was found for the partially impregnated catalyst at low palladium loading. A catalyst prepared by partial impregnation with high palladium loading unexpectedly only showed low conversion with an unknown cause. Catalysts prepared by melt infiltration with phenol and subsequent impregnation with the PdTA solution showed poor conversion. As it was initially expected that catalysts with blocked micropores would outperform catalysts with only impregnation into micropores, this was a surprising result. It is likely that catalyst deactivation occurs for these catalysts, however the mechanism of deactivation is unknown. A possibility is that Ostwald ripening or sintering is a cause for deactivation, or that adsorbed phenol from catalyst preparation (or a combination of these causes) is the reason for catalyst deactivation. It thus seems that particles confined in smaller particles show the highest catalytic activity, which may be due to the fact that particles confined in small pores show less tendency to grow during the catalytic reaction.

Chapter 5

Concluding remarks and outlook

In this work, we have studied a method to selectively impregnate porous carbon supports with pores ranging in size from micropores to macropores for palladium on carbon catalysts. By adjusting the impregnation volume, pores of different sizes can be selectively impregnated using a tetraamminepalladium solution. This was performed in a thermoporometry study by impregnating high surface area graphite HSAG500 with different amounts of the aqueous solution and measuring the resulting melting point of the pore water using DSC. Using TGA, the amount of liquid in the pores was then determined to obtain the extent of pore filling. After performing multiple experiments with different degrees of pore filling, a relationship was obtained between the maximum pore radius that is filled and the degree of pore filling. This showed that incomplete impregnation results in the impregnating liquid being present in the smallest pores available, with no liquid observed in larger pores. In order to selectively impregnate larger pores, experiments were performed in which a pore blocking agent was introduced to the porous carbon prior to adding the impregnating liquid. Several pore blocking agents were tried (toluene, cyclohexanol and phenol) using impregnation and melt infiltration. Both toluene and cyclohexanol impregnations gave poor results, however melt infiltration using phenol proved to be an easy to control addition method in the preparation set-up used. Subsequent impregnation with water showed a shift in melting temperature of the water towards higher temperatures in DSC. It was thus concluded that it is possible to selectively impregnate larger pores with water employing phenol as pore blocking agent, making use of capillary suction to first block small pores with subsequent impregnation using the impregnating liquid.

Different catalysts were then synthesized using the methods employed for selective impregnation with palladium weight loadings of 1 - 1.5% and 5% with a tetraamminepalladium solution as palladium precursor. Calculating the average particle size for different particles did not show a clear correlation between particle size and palladium weight loading. Particle size distributions did show a slightly larger proportion of larger particles being present when the weight loading of palladium was higher or when the catalyst was prepared by melt infiltration of phenol and subsequently impregnating with a PdTA solution, which is an indication that micropores and small mesopores may be blocked by phenol. However, the average palladium particle size was not much affected by this shift. TEM measurements from the spent catalysts showed no significant increase in the particle size. The only change observed was for the spent catalyst which was prepared with selective impregnation into the smaller pores, which showed a significant decrease in particle size, but no apparent cause was found for this behaviour.

Experiments with catalytic hydrogenation of cinnamaldehyde using these catalysts found that catalysts prepared by melt infiltration of phenol and subsequently impregnating with a PdTA solution significantly underperformed, not reaching full

conversion of cinnamaldehyde after 4 hours reaction time. This was surprising, as it was hypothesized that palladium particles in the more easily accessible large mesopores would show a higher activity. Instead, catalysts prepared by partial impregnation showed a 100% conversion of cinnamaldehyde, which was the same as catalysts prepared by full impregnation at both high and low palladium loading.
Calculations were performed on the initial rate of conversion of cinnamaldehyde by the various catalysts. Catalysts prepared with a low weight loading by full impregnation and partial impregnation showed the highest initial rate per gram of palladium present, which suggest a high catalytically active surface area is available. Interestingly, catalysts prepared by melt infiltration of phenol and subsequent impregnation with the PdTA solution showed a relatively low conversion rate which is consistent with the low final conversion of cinnamaldehyde obtained with these catalysts. The turnover frequency (TOF) was also determined for 3 samples, which interestingly showed a high TOF for a catalyst prepared with the intended micropore and small mesopore blocking, revealing a high initial TOF.
The differences found in the product distribution after hydrogenation can be fully explained by earlier studies showing that larger palladium particles selectively hydrogenate the aldehyde, forming cinnamyl alcohol and then hydrocinnamyl alcohol while smaller palladium particles show selectivity towards hydrogenation of the C=C bond, forming hydrocinnamyl aldehyde.
Catalysts prepared by partial impregnation show a higher selectivity towards hydrocinnamaldehyde formation than catalysts prepared by full impregnation at equal palladium loading. This suggests that catalysts prepared by partial impregnation contain smaller particles than catalysts prepared full impregnation, which may be caused by the presence of these particles in relatively small pores, where the palladium particles are relatively limited in their growth during catalyst preparation. Catalysts prepared by melt infiltration with phenol and subsequently impregnating with a palladium precursor showed low cinnamaldehyde conversion. This may be due to palladium particles primarily being present in larger pores as the micropores may be blocked by phenol during catalyst preparation. The palladium particles thus have more room to grow resulting in larger particles with a lower surface to bulk ratio. The slightly higher selectivity towards cinnamyl alcohol and hydrocinnamyl alcohol would agree with this determination, however such a definitive increase in particle size was not observed in TEM images.
Further experiments would need to be performed to definitively confirm the increase in palladium particle size for impregnation into larger pores. A possibility would be to perform hydrogenations with catalysts using supports of different uniform widths. This would allow for a more controlled study of the influence of pore size on particle size. Another option would be to use a more bulky alternative to cinnamaldehyde, though care must be taken that palladium can catalyse the hydrogenation of these molecules. The use of phenol as pore blocking agent seems to effectively block the micropores and small mesopores, though the location of palladium particles upon selective impregnation could not be confirmed. More work should thus be done to understand the influence of phenol on the adsorption of palladium in the carbon support pores and the location of palladium particles in pores must be confirmed. Similarly, the location of palladium particles must be confirmed for catalysts prepared by partial impregnation as the obtained results are not sufficient to conclude that partial impregnation leads to palladium particles in small pores. A possibility to study the location of palladium particles in the support may be found in a tomographic technique such as in focused ion beam-scanning electron microscopy (FIB-SEM). While in using this technique an entire catalyst grain can be

characterized, it is not ideal as the resolution may be too low to study the small pores present in the Pd/C catalyst. It was also considered that phenol may cause catalyst deactivation, but was not confirmed. The mechanism by which this may occur is not well understood and more work is needed to see if catalyst deactivation occurs by adsorption of the pore blocking agent. Another question to be answered is what happens to the pore structure during catalysis. The pore structure was only examined for the fresh support, but during catalysis the pore structure could become more open, which may influence the catalyst selectivity. A simple way to explore this is by thermoporometry, which was successfully employed to study the pore structure of the fresh support.

Bibliography

(1) White, R. J.; Luque, R.; Budarin, V. L.; Clark, J. H.; Macquarrie, D. J. *Chem. Soc. Rev.* **2009**, *38*, 481–494.

(2) Felpin, F. X.; Ayad, T.; Mitra, S. Pd/C: An old catalyst for new applications - Its use for the Suzuki-Miyaura reaction., June 2006.

(3) Mori, A.; Miyakawa, Y.; Ohashi, E.; Haga, T.; Maegawa, T.; Sajiki, H. *Organic Letters* **2006**, *8*, 3279–3281.

(4) Vilches-Herrera, M.; Werkmeister, S.; Junge, K.; Börner, A.; Beller, M. *Catalysis Science & Technology* **2014**, *4*, 629.

(5) Ley, S. V.; Stewart-Liddon, A. J. P.; Pears, D.; Perni, R. H.; Treacher, K. *Beilstein Journal of Organic Chemistry* **2006**, *2*, 15.

(6) Dormán, G.; Kocsis, L.; Jones, R.; Darvas, F. *Journal of Chemical Health and Safety* **2013**, *20*, 3–8.

(7) Sarioğlan, Ş. *Platinum Metals Review* **2013**, *57*, 289–296.

(8) Toebes, M. L.; van Dillen, J. A.; de Jong, K. P. *Journal of Molecular Catalysis A: Chemical* **2001**, *173*, 75–98.

(9) Bitter, J. H.; van der Lee, M. K.; Slotboom, A. G. T.; van Dillen, A. J.; de Jong, K. P. *Catalysis Letters* **2003**, *89*, 139–142.

(10) Van der Lee, M. K.; van Dillen, A. J.; Bitter, J. H.; de Jong, K. P. *Journal of the American Chemical Society* **2005**, *127*, 13573–13582.

(11) Bezemer, G. L.; Radstake, P. B.; Koot, V.; Van Dillen, A. J.; Geus, J. W.; De Jong, K. P. *Journal of Catalysis* **2006**, *237*, 291–302.

(12) De Jong, K. P., *Synthesis of Solid Catalysts*; WILEY-VCH Verlag GmbH: 2009.

(13) Jiao, L.; Regalbuto, J. R. *Journal of Catalysis* **2008**, *260*, 329–341.

(14) Deacon, H. US Patent 85370., 1868.

(15) Lekhal, A.; Glasser, B. J.; Khinast, J. G. *Chemical Engineering Science* **2001**, *56*, 4473–4487.

(16) Zhu, X.; Cho, H. R.; Pasupong, M.; Regalbuto, J. R. *ACS Catalysis* **2013**, *3*, 625–630.

(17) Vanyorek, L.; Halasi, G.; Pekker, P.; Kristály, F.; Kónya, Z. *Catalysis Letters* **2016**, *146*, 2268–2277.

(18) Gurrath, M.; Kuretzky, T.; Boehm, H. P.; Okhlopkova, L. B.; Lisitsyn, A. S. *Fuel and Energy Abstracts* **Nov. 2000**, *41*, 368–369.

(19) Matos, I.; Fernandes, S.; Guerreiro, L.; Barata, S.; Ramos, A. M.; Vital, J.; Fonseca, I. M. *Microporous and Mesoporous Materials* **2006**, *92*, 38–46.

(20) Den Brave, D.; Lamme, W. S.; de Jongh, P. E.; de Jong, K. P. Bachelor ' s Thesis Investigating the Behaviour of Water in Porous Carbons Using Differential Scanning Calorimetry., 2016.

(21) Nagendiran, A.; Pascanu, V.; Bermejo Gómez, A.; González Miera, G.; Tai, C. W.; Verho, O.; Martín-Matute, B.; Bäckvall, J. E. *Chemistry - A European Journal* **May 2016**, *22*, 7184–7189.

(22) Kuijpers, C.; Huinink, H.; Tomozeiu, N.; Erich, S.; Adan, O. *Chemical Engineering Science* **2017**, *173*, 218–229.

(23) Riikonen, J.; Salonen, J.; Lehto, V. P. *Journal of Thermal Analysis and Calorimetry* **2011**, *105*, 1811–1821.

(24) Yang, D.; Jiao, L.; Zhang, B.; Du, G.; Lu, Y. *Journal of Pharmaceutical and Biomedical Analysis* **June 2017**, *140*, 169–173.

(25) Schmidt, R.; Hansen, E. W.; Stocker, M.; Akporiaye, D.; Ellestad, O. H. *Journal of the American Chemical Society* **1995**, *117*, 4049–4056.

(26) Veselá, P.; Riikonen, J.; Nissinen, T.; Lehto, V.-P.; Slovák, V. *Thermochimica Acta* **2015**, *621*, 81–89.

(27) Schreiber, A.; Ketelsen, I.; Findenegg, G. H. *Physical Chemistry Chemical Physics* **2001**, *3*, 1185–1195.

(28) Yamamoto, T.; Mukai, S. R.; Nitta, K.; Tamon, H.; Endo, A.; Ohmori, T.; Nakaiwa, M. *Thermochimica Acta* **2005**, *439*, 74–79.

(29) Nagpure, A. S.; Gurrala, L.; Gogoi, P.; Chilukuri, S. V. *RSC Adv.* **2016**, *6*, 44333–44340.

(30) Jiang, F.; Cai, J.; Liu, B.; Xu, Y.; Liu, X. *RSC Adv.* **2016**, *6*, 75541–75551.

Appendix A

TGA analysis method

When a porous (carbon) support is impregnated with water, the mass of the water impregnated per mass of the support can be easily obtained from TGA. The only requirement to obtain a clear result is that the temperature of the TGA oven is sufficient to evaporate any water present in the sample but not so high that it may degrade the support. It is of course also important that the water must have a way to be evacuated from the sample. As the samples measured with TGA are typically first analysed with DSC, requiring a hermetic seal on the pan, the lid on the sample pan can be pierced using a needle. From this, the degree of pore filling can be obtained from the mass loss due to evaporation of water and mass of the support via Equation 3.7.

Tracking of tetraamminepalladium decomposition using TGA When impregnating a support with the PdTA precursor, $(NH_3)_4Pd(NO_3)_2$, the mass fractions of Pd, NH_3 and NO_3 in the solution have to be taken into account when calculating the impregnation volume. An example of a TGA thermogram is shown in Figure A.1. In this example, HSAG 500 was impregnated using a tetraamminepalladium nitrate solution. It was found that $(NH_3)_4Pd(NO_3)_2$ decomposes almost completely upon

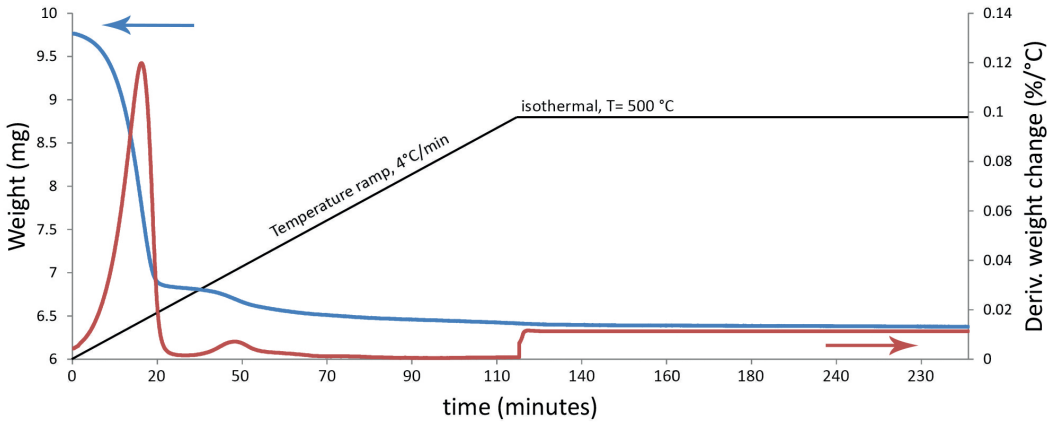

Figure A.1: TGA thermogram of porous carbon support HSAG500 impregnated with 5 wt.% PdTA solution. The blue line represents the decrease in weight of the sample over time. The red line is the derivative of the weight change with respect to the temperature change. Note the jump in the derivative at 116 minutes, caused by the switch of the TGA mode from temperature increase to an isotherm, all points in the derivative after this time can thus be neglected.

heating at a temperature above 200 °C. By assuming the concentration of the PdTA complex in water after impregnation is the same as the fresh PdTA solution and assuming complete decomposition of the complex, a good approximation can be made

of the total PdTA solution present in the HSAG pores prior to performing TGA.
To calculate the mass of $(NH_3)_4Pd(NO_3)_2$ impregnated into the support the simplification was made that prior to heating of the sample, the palladium complex had not undergone any reaction with the support or functional groups thereof and that upon evaporation under a N_2 flow only the central palladium atom remains. This offers a base for further calculations as we may now assume that NH_3 and NO_3 at some point will need to decompose and evaporate. From the TGA thermogram, a distinct evaporation curve could be seen that was not present when performing TGA on water-impregnated carbon supports.
Calculating the derivative weight change, the start and end point of evaporation of the second peak were taken as the minimum in the derivative of the weight change. Considering the mass fraction of NH_3 and NO_3 from $((NH_3)_4Pd(NO_3)_2)$ is 0.643546, the total mass of Pd in the sample could be estimated via the formula $m_{\text{Pd}} = \Delta m \cdot [\text{Pd}]/([\text{NH}_3] + [\text{NO}_3]) = \Delta m \cdot 0.356454/0.643546$. A possible error may be introduced using this method due to the fact that the end product is taken as pure Pd while some palladium oxide may be present. The oxygen needed to form these complexes may come from the support, or any remaining water in the pores. However, it is unknown whether this palladium oxide is present and the possibility of its potential presence is thus ignored in the calculations. The calculation method thus offers a way to calculate the amount of the solvent-free tetraamminepalladium complex present upon impregnation of the support.
It is emphasized that any amounts or weight loadings of palladium reported in this work were not obtained through TGA, as this was considered as unreliable. This is primarily because of the simplifications made to perform the calculations, as outlined in this appendix, but also because the sample taken for TGA is very small (commonly between 5-8 mg). This means that only the local palladium loading for the (small) sample can be determined, which may be an indication of the palladium loading, but if the palladium distribution is not completely homogeneous over the entire catalyst the calculated palladium loading for the sample may deviate from the overall palladium loading. Instead, only calculated amounts were reported based on the concentration of the tetraamminepalladium solution used and the amount thereof impregnated into a porous support. The results obtained via the method described here do however corroborate the calculated Pd-loadings on the support.

Thermogravimetric analysis of phenol and water containing samples In order to determine the amounts of phenol and water in a sample of porous carbon a similar TGA method was used. As can be seen in Figure A.2 two distinct weight changes occur. The first was attributed to water and the second to phenol as water has the lower boiling point of 100 °C. The onset of the second weight change was taken as the first minimum in the derivative weight change. It was assumed that at this point all water had evaporated and evaporation of phenol could start to occur. This allows for the approximation of the amount of phenol and water in the sample. This method is not entirely exact, as a small overlap in evaporation can occur. The first weight change (up to the first minimum of the derivative of the weight change with the change in temperature) is thus taken as the amount of water impregnated and the second weight change as the amount of phenol impregnated, starting at the minimum of the derivative of the weight change. The obtained values for the amount of water and phenol in the sample can then be converted to the degree of pore filling of water ϕ_{water} and phenol ϕ_{PB} via the Equation 3.7, which added together form the total degree of pore filling ϕ_{total}.

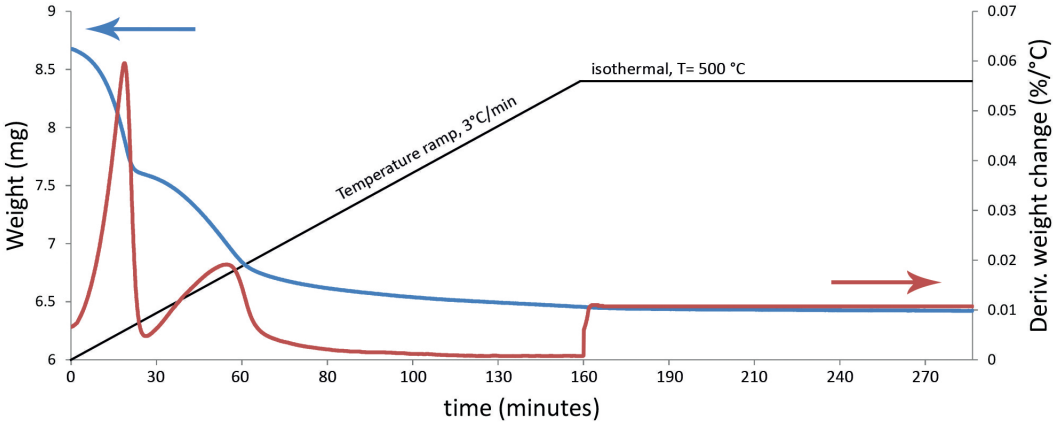

Figure A.2: TGA of a sample containing water and phenol. The blue line is the total weight, the red line the derivative of the weight change with respect to the change in temperature. At 160 minutes a jump can be seen in the derivative of the weight change, caused by the switch of the TGA mode from temperature increase to an isotherm, all points in the derivative after this time can thus be neglected.

Appendix B

DSC Freezing curves

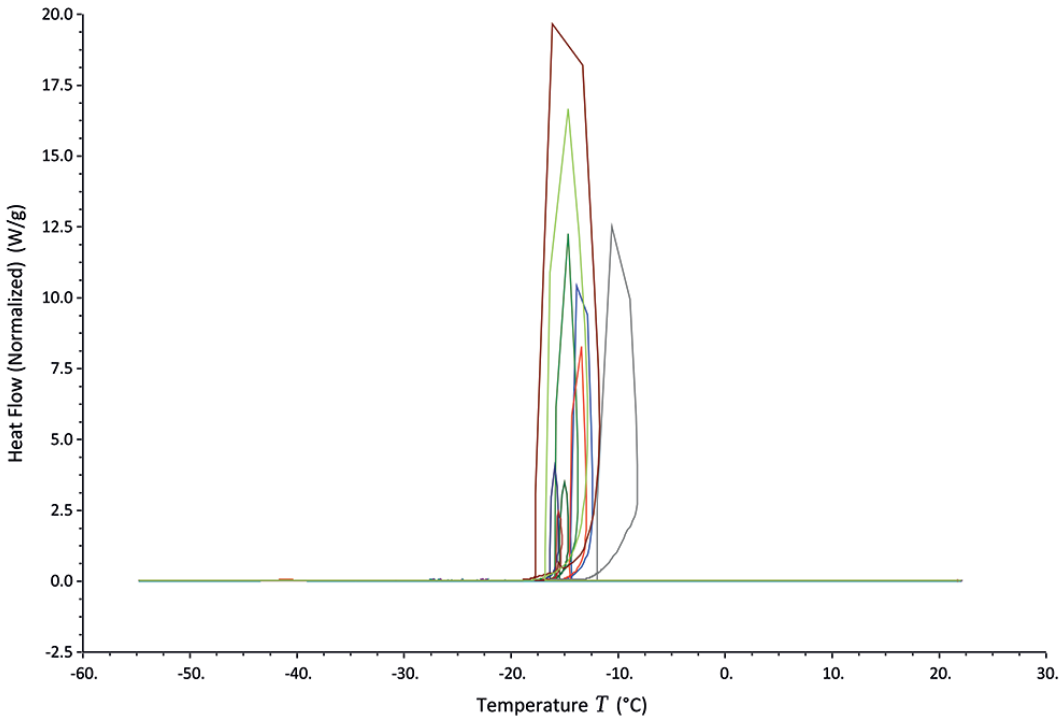

Figure B.1: DSC curves for the freezing of the precursor solution in samples impregnated to varying extends. Scan direction was from right to left at a rate of 1 °C per minute.

Appendix C

Spent catalysts TEM images

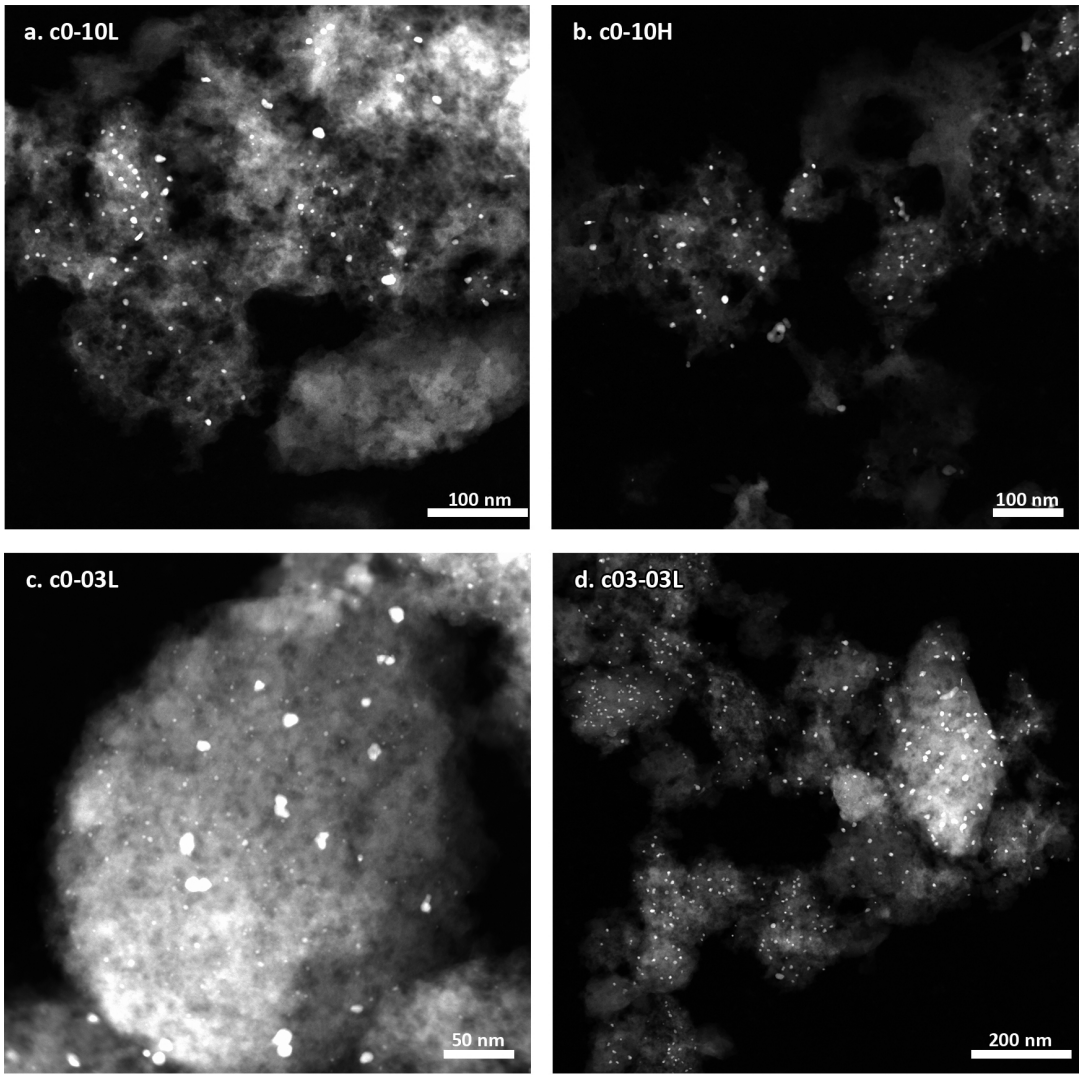

Figure C.1: STEM images of spent catalysts from (**a**) catalyst c0-10L, (**b**) catalyst c0-10H, (**c**) catalyst c0-03L, (**d**) catalyst c03-03L.

Appendix D

Pd particle size distributions

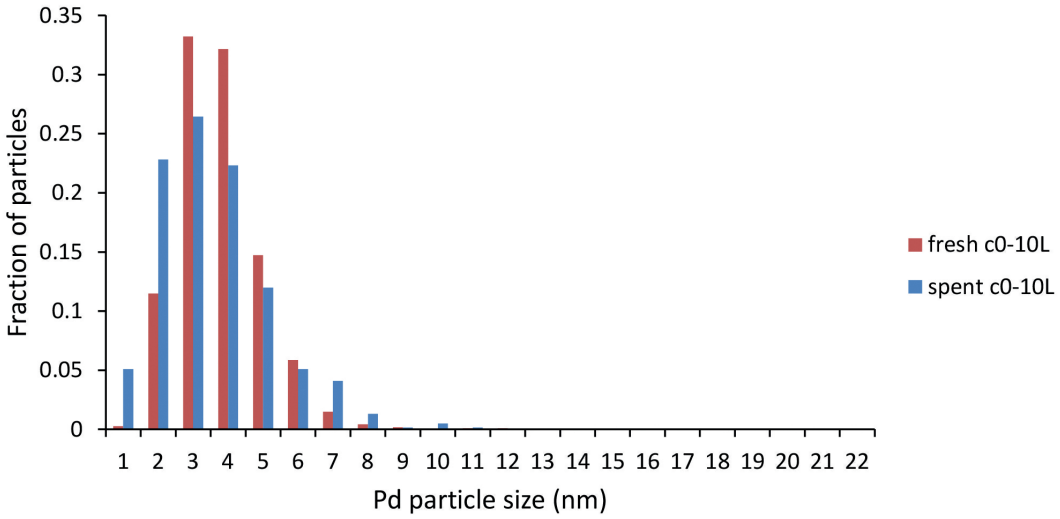

Figure D.1: Particle size distribution for fresh (red) and spent (blue) catalyst c1. The denoted particle size is in the range $\pm$ 0.5 nm.

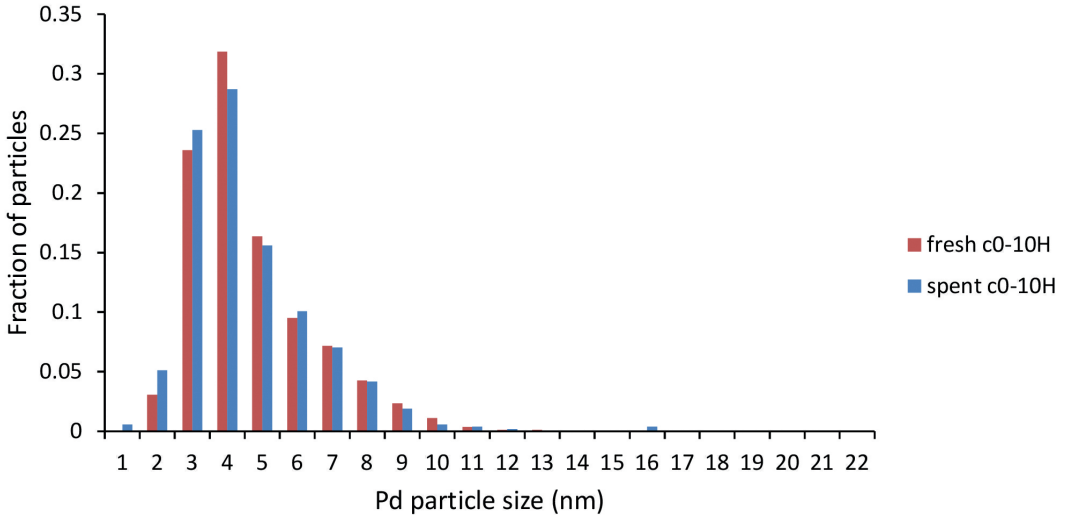

Figure D.2: Particle size distribution for fresh (red) and spent (blue) catalyst c2. The denoted particle size is in the range $\pm$ 0.5 nm.

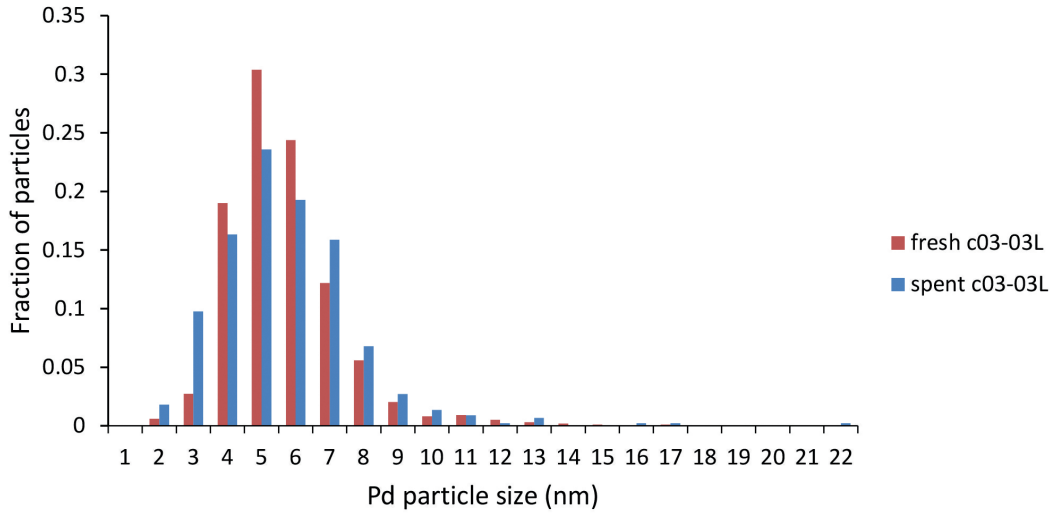

Figure D.3: Particle size distribution for fresh (red) and spent (blue) catalyst c5. The denoted particle size is in the range $\pm$ 0.5 nm.